CERN-ACC-2017-0088
rogelio.tomas@cern.ch

Optics Measurement and Correction Challenges for the HL-LHC

F. Carlier, J. Coello, S. Fartoukh, E. Fol, D. Gamba,
A. García-Tabares, M. Giovannozzi, M. Hofer, A. Langner,
E.H. Maclean, L. Malina, L. Medina, T.H.B. Persson,
P. Skowronski, R. Tomás, F. Van der Veken
and A. Wegscheider.
CERN, Geneva, Switzerland.

Abstract

Optics control in the HL-LHC will be challenged by a very small β^* of 15 cm in the two main experiments. HL-LHC physics fills will keep a constant luminosity during several hours via β^* leveling. This will require the commissioning of a large number of optical configurations, further challenging the efficiency of the optics measurement and correction tools. We report on the achieved level of optics control in the LHC with simulations and extrapolations for the HL-LHC.

Geneva, Switzerland
November 10, 2017

Contents

1 Introduction

LHC has demonstrated an unprecedented optics control for high energy colliders, down to the 1% level in β-beating [1, 2, 3, 4, 5, 6] and $|C^-| = 2 \times 10^{-4}$ in coupling [7, 8, 9]. The high luminosity upgrade of the LHC (HL-LHC) [10] will challenge the efficiency and accuracy of optics measurement and correction algorithms in many ways:

1. About 50 different optics will need to be finely commissioned for physics production. A simulated HL-LHC physics fill is shown in Fig. 1 (details

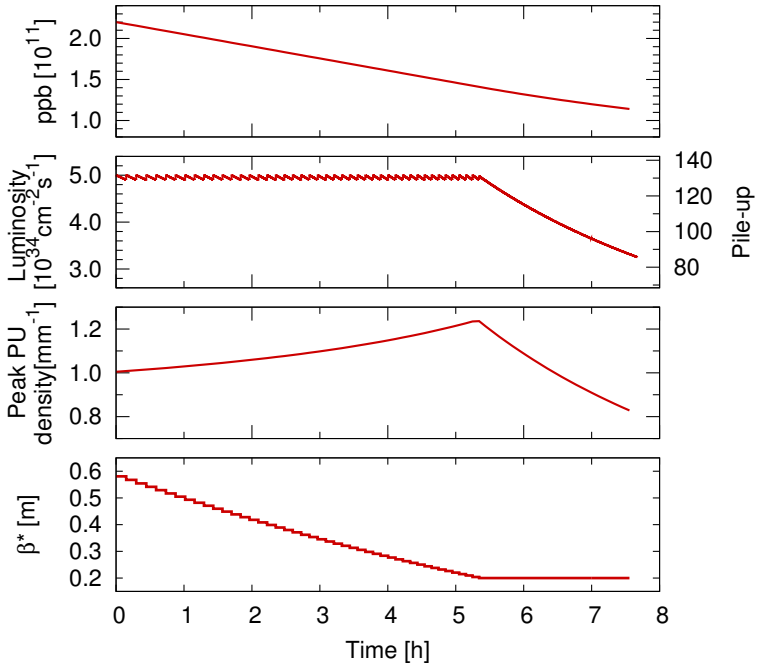

Figure 1: Simulated evolution of an HL-LHC physics fill with baseline parameters.

can be found in [11, 12, 13]). The sawtooth pattern in the instantaneous luminosity reflects the step-wise changes in β^* to restore luminosity after a 2% decay.

2. β^* measurement accuracy is limited by tune ripple when applying the K-modulation technique [14]. This triggered the following requests and improvements:
   - A new powering scheme with one main power converter for the full triplet.
   - A new trim circuit powering only one quadrupole of the Q1 assembly, Q1A [15].
   - Possibly improved current jitter performance for the four main dipole circuits in the telescopic arcs [16].
   - The development of an optics-measurement-based BPM calibration to boost the accuracy of the β from amplitude tehcnique in the HL-LHC Interaction Regions (IRs).
3. Local corrections in the IRs will be significantly more constrained in HL-LHC than in LHC as the β functions at the crab cavities should be controlled with similar accuracy as the β^*.

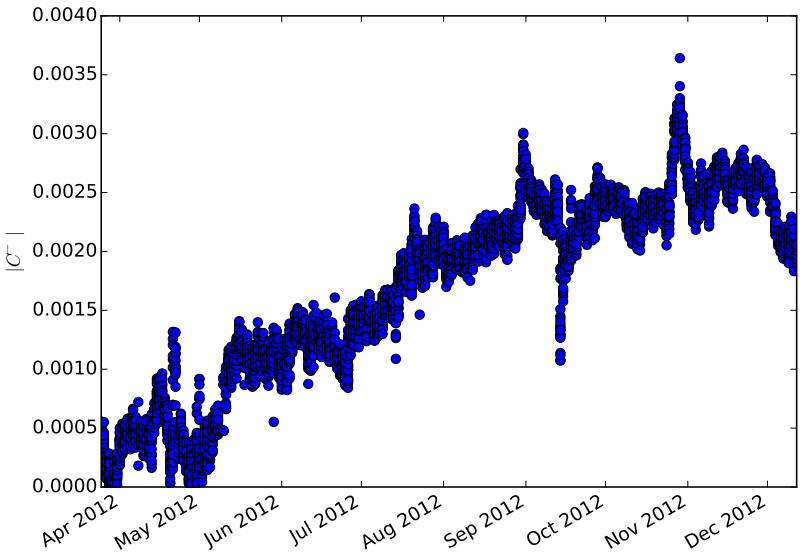

Figure 2: Inferred contribution from measured triplet tilts to $|C^-|$ versus time in 2012 with $\beta^* = 60$ cm in the LHC.

4. Sensitivity of transverse coupling to ground motion in the IRs will be highly increased, requiring frequent adjustments. Figure 2 shows the inferred contribution from measured triplet tilts to $|C^-|$ in the 2012 LHC run. We expect a factor 4 enhancement for the HL-LHC, i.e. $\Delta|C^-| \approx 0.012$ after 7 months. In HL-LHC $|C^-|$ has to be corrected down to 0.001 to avoid instabilities [17].

5. For HL-LHC the non-linear errors in the IR in combination with the crossing angles give up to 20% peak β-beating. This is well above tolerances for machine protection and requires a totally new approach to optics commissioning since crossing angles were never applied during LHC optics commissioning. In 2016 optics were measured with crossing angles 3 months after commissioning. The measured shift in the β-beating is about 3%, see Fig. 3. This might affect luminosity imbalance between the 2 detectors in the LHC and first steps to address this were taken in the 2017 LHC optics commissioning [18].
6. In HL-LHC the IR non-linear correction up to dodecapole order is required to restore about 5σ of dynamic aperture (DA), see Section 9.1. Procedures to guarantee the successful IR non-linear commissioning are still under development [19].

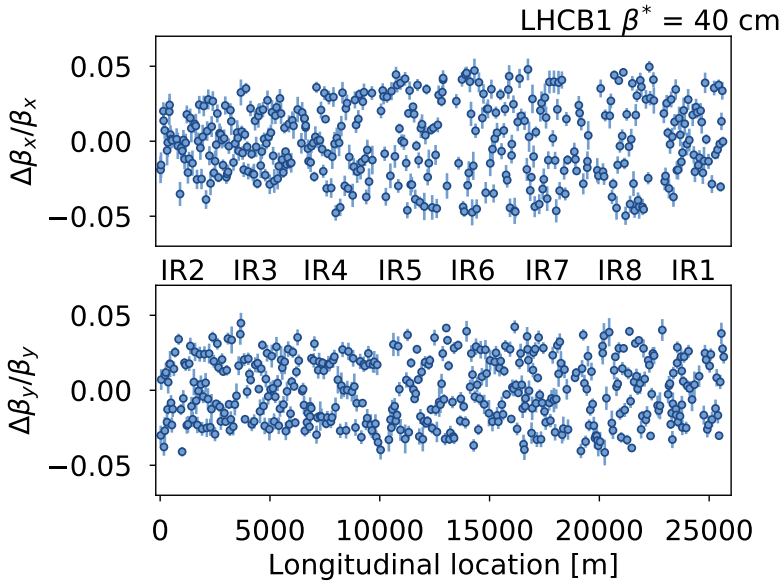

Figure 3: Difference of the β-beating from two measurements with and without crossing angles in LHC at $\beta^* = 40$ cm in 2016. Horizontal (top) and vertical (bottom) β-beating are shown. The two measurements, with and without crossing angles, were separated by 3 months.

7. Head-on and long-range beam-beam interactions are a source of sizeable β-beating in HL-LHC [20]. At the start of the fill we expect a 13% peak β-beating in HL-LHCV1.3 as shown in Fig. 4. This affects luminosity imbalance between the two main detectors and possibly machine protection. Possible diagnostics and correction schemes are being investigated [21, 22].

The contents of the report are as follows. Section 2 describes how LHC achieved the 1% rms β-beating level. Section 3 reports on the limitations of the current N-BPM method to measure β functions for the HL-LHC optics and its development into a more robust and faster algorithm by using analytical equations. Section 4 studies the performance of optics corrections including only arc erros in the ATS optics [23]. The expected resolution of the K-modulation technique with updated power converter performance estimates is given in Section 5. Section 6 reports on the achieved performance of the optics-measurement-based BPM calibration. IR local optics and coupling corrections are studied in Section 7 for the HL-LHC via realistic simulations. The potential of having effective models of the machine is highlighted in Section 8. Section 9 studies the impact of IR non-linearities in dynamic aperture, machine operation, linear optics and beam dynamics together with potential correction methods.

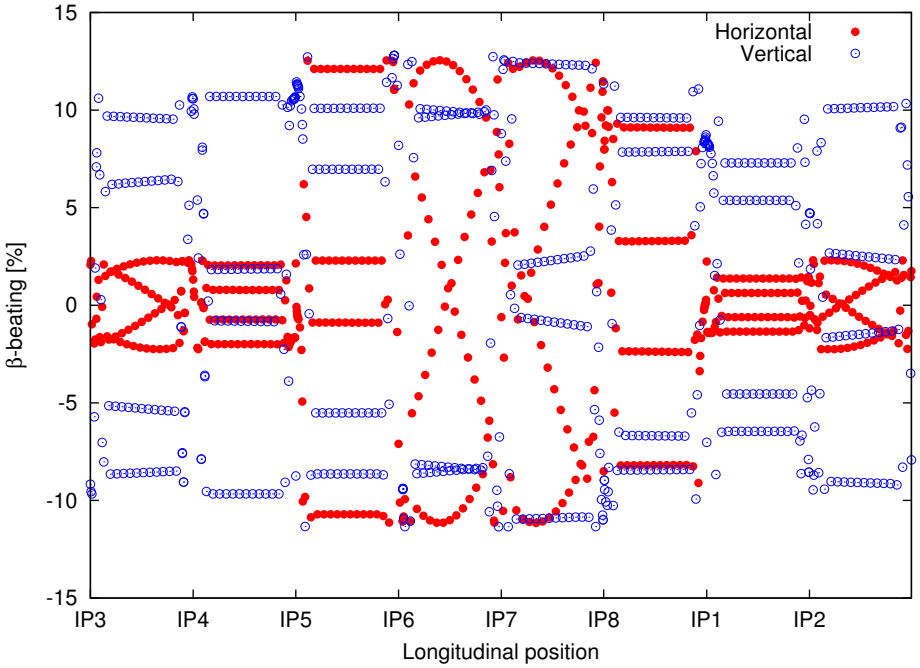

Figure 4: β-beating from head-on and long-range beam-beam in HL-LHCV1.3 baseline configuration at the start of the fill.

2 How LHC achieved below 2% rms β-beating

The 2012 optics commissioning of the LHC reached a new record low β-beating for hadron colliders [4]. Since then, many new improvements have been made to equipment, algorithms and analyses to further reduce the errors and uncertainties of the optics measurements and corrections. Improvements to the reconstruction of both the β functions and the coupling from turn-by-turn data have been made [5, 6, 7, 8]. A new online K-modulation application has also been developed, which enables direct measurement of the β^* [24].

In 2015 orbits were subject to fast drift with periodicity of approximately 8 h [25] due to the movements of the triplet quadrupoles in IP8. This significantly reduced the accuracy of dispersion measurements and global corrections. During the 2016 winter shutdown the reason of the movement was traced back to cryogenics pressure and temperature regulation and an adequate stabilization system was introduced [25]. These orbit drifts were not observed in 2016.

The AC-dipole was upgraded during the first long shut down to excite the beam from 2200 to 6600 turns. The performance was further improved in 2016 thanks to the replacement of the Beam 1 amplifier that previously caused a tune variation in the driven frequency [26, 6].

In 2015 it was found out that there was a systematic offset towards the focusing quadrupole of the β^* waists in both IP1 and IP5 resulting in an increase of the β^*, causing about 5% luminosity loss [27, 28, 29]. This was unexpected for triplet gradient errors below 0.04% rms (WISE [30, 31]). Nevertheless, triplet gradient errors up to 0.11% were expected in [32]. A test of the significance was done. The magnetic uncertainty is set to 0.11% rms and the assumption is that the corrections are reproducing the errors, giving a p-value of 0.04. This suggests that the optics errors in the IRs are not well represented by the 0.11% rms uncertainty in the triplet quadrupole gradients. Already during the ion optics commissioning in 2015 additional corrections were performed to mitigate this issue [29]. The tool for K-modulation measurements was then further improved and fully automatized to obtain the result online for corrections [33, 14].

2.1 Improvements in β-function and K-modulation measurements

A new method to calculate the β functions from the phase advances was developed. The previous method used 3 BPMs [34] while the N-BPM method [5] uses 11 BPMs in the case of the LHC. This significantly reduces the error bars on the measured β functions and provides a more accurate uncertainty. The optics model used to reconstruct the β function has been improved by including the settings of the tune corrector magnets [35, 36].

K-modulation [37, 24] is performed using the two closest quadrupoles to the IP, providing a measurement of β^* and waist [37, 38, 14]. The online implementation of the K-modulation tool allows for a faster and more accurate measurement of β^*. K-modulation measurements are done at nominal injection tunes ($Q_x = 64.28$, $Qy = 59.31$) which are further away from third order and coupling resonances than the collision tunes ($Q_x = 64.31$, $Q_y = 59.32$). A cleaning tool has been developed to clean outliers in the tune data online. The domain of acceptance is determined by tracing a parallelogram around the desired data, as illustrated in Fig. 5. This has been a crucial ingredient for online accurate measurements and corrections.

2.2 Local and global corrections

Local corrections are applied in the IRs using the segment-by-segment technique [4]. These are evaluated for both beams and for several optics in order to constraint the correction. Furthermore, since 2016 the β functions obtained from the K-modulation are also included in the segment-by-segment technique. Figure 6 shows how the 2015 and 2016 correction both correct the phase beating but it is only the 2016 correction that reproduces the β^* and waist shift.

The local corrections reduced the β-beating to a peak of about 20%. However,

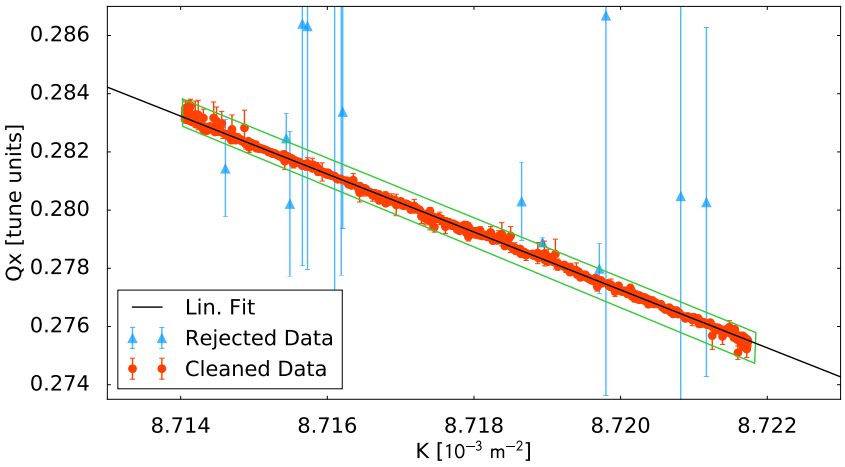

Figure 5: Horizontal tune versus triplet strength for Beam 2. The rejected data is shown in blue. An online tool is used to specify the domain of acceptance shown in green.

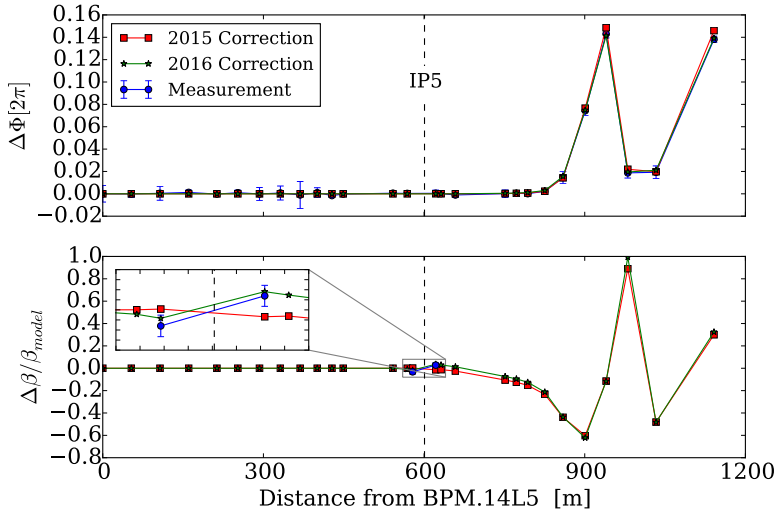

Figure 6: A comparison between how well the 2016 and 2015 corrections would correct the phase error (on top) and the local β-beating (bottom). The red line shows the 2015 correction, the green 2016 and the blue shows the measurement. Note that both the lines and points show the deviation from the ideal model.

Year	Beam	$\Delta\beta_x/\beta_x$ [%]	$\Delta\beta_y/\beta_y$ [%]	$\Delta D_x/\sqrt{\beta_x}$ [$\sqrt{m}$]
2015	1	3.2	1.7	0.8
	2	4.2	2.0	1.2
2016	1	1.4	1.3	0.5
	2	1.8	1.4	0.6

Table 1: rms β-beating and normalized dispersion error in 2015 and 2016 for both beams and planes.

to reach a lower β-beating a global correction approach is needed. This is needed since not all the errors are originating from the IRs. The better corrections also provide more margin for other errors in the machine and reduce the luminosity imbalance between the experiments. The global correction is based on a response matrix approach. The correction method was improved in 2016 by taking the measurement uncertainties into account as weights and including β functions from K-modulation. Additionally weights are used, e.g. giving a higher weight to the β functions close to the IP than to the phase advance [39]. To find a good trade-off among the observables, corrections are evaluated with online simulations before they are applied to the machine.

After local and global corrections in 2016 an unprecedented rms β-beating below 2% was achieved in 2016 for both beams, see Table 1. Figure 7 illustrates the β-beating for Beam 1 at β^* of 40 cm. The final results have been filtered from malfunctioning BPMs [40, 41]. Even more importantly than the reduction of the overall β-beating is the improved control of β^*. Table 2 shows the measured β^* before and after the different corrections. The final β^* accuracy is below 1%. Figure 8 shows the evolution of the average β^* waist for 2015, proton and ion runs, and 2016.

The LHC optics has been successfully commissioned down to $\beta^* = 40$ cm at 6.5 TeV, which is lower than the design value of 0.55 m at 7 TeV. An unprecedented β-beating in a high energy proton collider has been achieved. In particular a control about 1% has been demonstrated for the β^*.

3 N-BPM method for HL-LHC

The original method to determine the beta function from turn-by-turn data uses three adjacent BPMs [42], but the reliability of this method depends on the phase advance between the BPMs. If they are close to a multiple of π, measurement errors are strongly enhanced. To avoid bad combinations and to increase statistics, a new method was developed in [5] which uses several combinations of 3

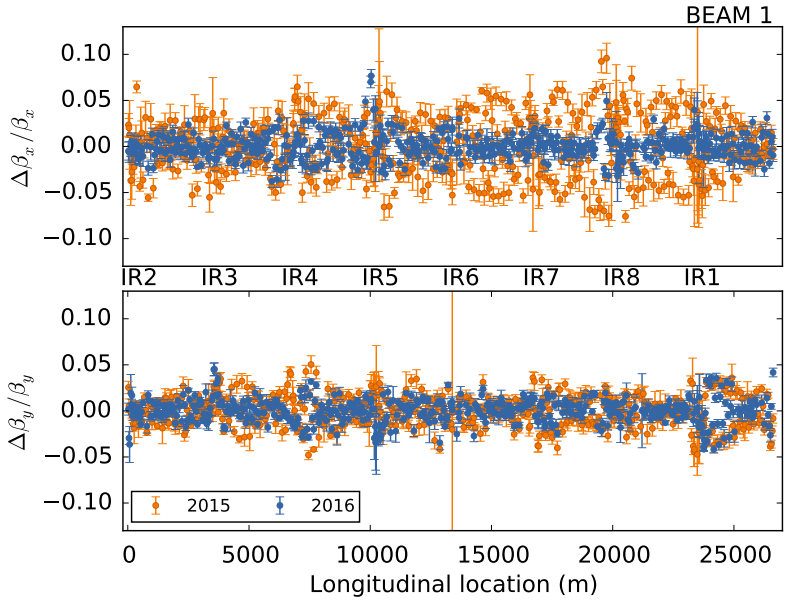

Figure 7: Comparison of β-beating after local and global corrections around the ring in 2015 and 2016 at $\beta^* = 40$ cm for Beam 1.

	IP 1 β^* [cm]			
	Beam 1		Beam 2	
	H	V	H	V
Before Corr	62.3 ± 1.2	73.1 ± 1.0	41.7 ± 1.3	75.4 ± 3.0
After Local	41.2 ± 0.3	40.9 ± 0.1	36.6 ± 0.1	40.4 ± 0.4
After Global	39.8 ± 0.5	40.1 ± 0.1	39.8 ± 0.1	40.1 ± 0.1
	IP 5 β^* [cm]			
	Beam 1		Beam 2	
	H	V	H	V
Before Corr	48.0 ± 0.8	30.9 ± 0.1	45.8 ± 0.2	45.0 ± 0.8
After Local	35.7 ± 0.2	40.9 ± 0.2	40.4 ± 0.3	40.4 ± 0.1
After Global	39.9 ± 0.2	40.1 ± 0.1	39.5 ± 0.1	39.6 ± 0.2

Table 2: The measured β^* before correction, after local correction and after global corrections for the $\beta^* = 40$ cm optics.

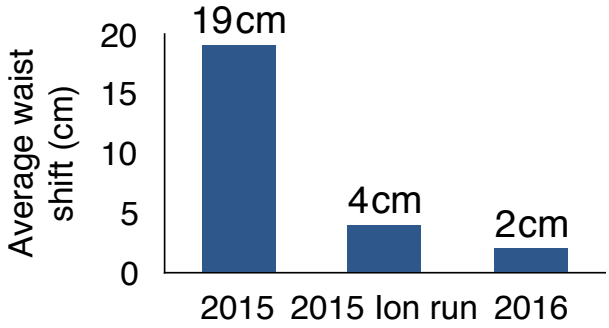

Figure 8: The average shift of the waist of the β function at IP1 and IP5 for the $\beta^* = 40$ cm optics.

BPMs, the N-BPM method. However, since systematic errors accumulate along the lattice, taking BPMs separated by large distances gives less precise results. To account for this a weighted average is used that includes lattice uncertainties. In comparison to the three BPM method, there is a huge gain in precision in the IRs, where neighbouring BPMs have bad phase advances with respect to each other.

However the N-BPM method relies on lengthy Monte Carlo simulations that present complications in the pushed HL-LHC optics when lattice errors make the lattice unstable. Also, ATS arc optics has exactly π phase advance every two cells making measurements challenging even for the N-BPM method. A new method is introduced here which uses analytical calculation of the systematic errors and applies a filter on the BPM combinations. It improves the N-BPM method in terms of computation speed, accuracy and stability.

3.1 Analytical N-BPM method and a first application to ATS optics

The analytical N-BPM method uses the results of [43] to analytically calculate the propagation of systematic errors. If one knows the quadrupole field errors of the lattice elements, the β function can be computed by [43]

$$\beta_1 = \frac{\cot\phi_{12} - \cot\phi_{13}}{\cot\phi_{12}^{\mathrm{m}} - \cot\phi_{13}^{\mathrm{m}} - (h_{12} + h_{13})}\beta_1^{\mathrm{m}} , \tag{1}$$

$$h_{ij} = \sin^{-2}\phi_{ij}^{\mathrm{m}} \sum_{i<w<j} \beta_w^{\mathrm{m}} \sin^2\phi_{wj}^{\mathrm{m}} \delta K_{1w} . \tag{2}$$

Parameters with superscript m are model values, $\phi_{ij} = \phi_j - \phi_i$ is the measured phase advance, δK_{1w} is the quadrupolar field error and the sum runs over all elements w between i and j. Since sextupole transversal misalignments and quadrupole longitudinal missalignments introduce quadrupolar errors, they can

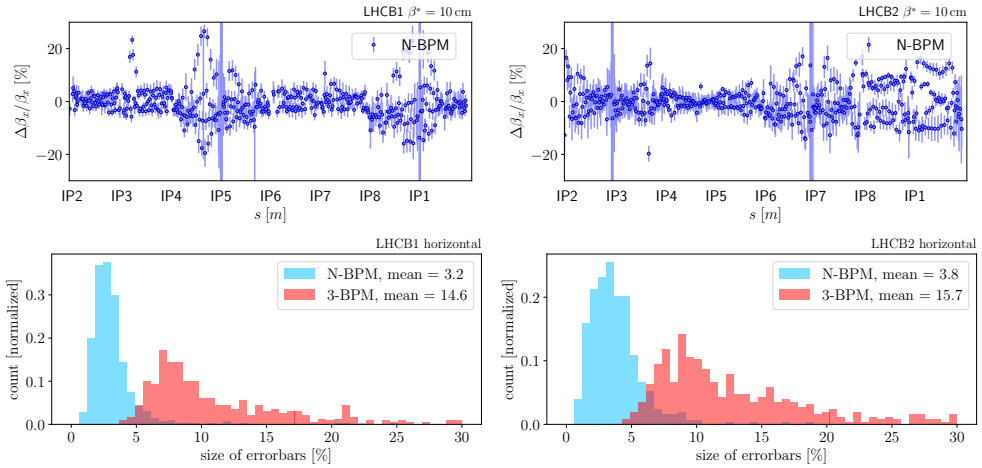

Figure 9: The upper plots show the horizontal β-beating at $\beta^* = 10\,\text{cm}$ for both beams, measured in 2016. The bottom plots show a comparison of the error bars of the β functions acquired by the 3-BPM method and the analytical N-BPM method, respectively. Error bars which are larger than 75% were ignored in the calculation of the average. The left plots are for Beam 1 and the right ones are for Beam 2.

be incorporated into the method. This equation is being extended to also include BPM longitudinal misalignments [44].

During the ATS optics MD in October 2016 [45, 46] the weighted average yielded some unphysical β values, originating from BPM combinations with phase advances $\phi_{ij} \approx n\pi$. As a solution, a filter for bad phase advances was introduced into the analytical N-BPM method. This allowed us to still use several combinations but skipping those which are numerically unstable. With these filters active, the measurement points could be restored everywhere in the lattice except for IR2 and IR5. Figure 9 shows the measured β-beating for the $\beta^* = 10\,\text{cm}$ optics of Beam 1. As a side effect, taking less combinations results in a lower computation time.

The Monte Carlo simulations failed for low β^* optics and the original N-BPM method could not be used during ATS MDs. This represents another advantage of the analytical N-BPM method, which computes systematic errors without resorting to simulations.

3.2 Preparing for 2017 measurements and HL-LHC

In HL-LHC about 50 optics will be used durig β^* leveling. The analytical N-BPM method will allow us to react quickly during measurements. Since the analytical

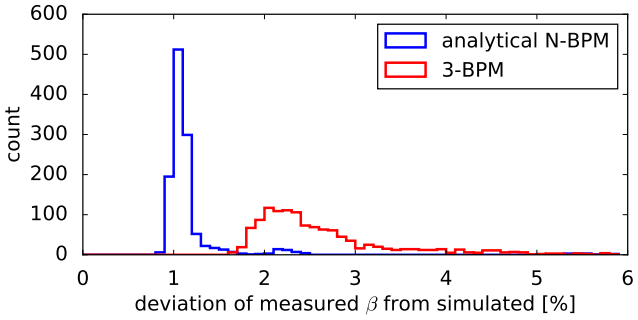

Figure 10: Simulations comparing 3-BPM and analytical N-BPM method for the HL-LHC. The figure shows histograms of the deviations of either of the methods from the simulated data.

N-BPM method takes as input just the optics parameters, even replacing the model does not affect calculation times. Since we can now skip the step of producing statistics with the Monte Carlo simulations, the time consumption of the total process including both planes, both beams and phase calculations was reduced to about 2 minutes on the computer that is used during measurement. Furthermore the code for calculating the β functions has been parallelized which again reduces the total analysis time to less than 40 s. The Monte Carlo simulations took 30 to 60 min with low statistics.

Simulations with the HL-LHC lattice demonstrate that the analytical N-BPM method yields better and more stable results than the 3-BPM method. This is illustrated in Fig. 10. The analytical N-BPM is being further developed [44].

4 Correcting arc errors in the HL-LHC

The impact of optics perturbations in the arc and their correctability is simulated for the HL-LHC in comparison to the LHC. For the HL-LHC simulation, the lattice and optics version HLLHCV1.1 is used [47]. The assumed quadrupole field errors are listed in Table 3 and furthermore 60 random sets of the b_2 uncertainty of the main dipoles are provided from WISE [31]. At the time of the study longitudinal alignment accuracy was not well known and a moderately low uncertainty of 1 mm is assumed for all quadrupole magnets and 1 cm for lattice sextupole. Additionally, for the sextupole magnets a transverse alignment uncertainty of 1 mm is considered. For the HL-LHC, additionally the following error tables are used for the b_2 uncertainty of IR dipole magnets, *D2_errortable_v5_spec*, *MBH_errortable_v1* and *D1_errortable_v1_spec* [48]. Global optics corrections

Table 3: Assumed rms gradient errors of different quadrupole magnet families.

Quadrupole family	**Error relative to the main field** (10^{-4})	**Quadrupole family**	**Error relative to the main field** (10^{-4})
MQ	18	MQYY	10
MQM	12	MQW	15
MQY	8	MQT	75

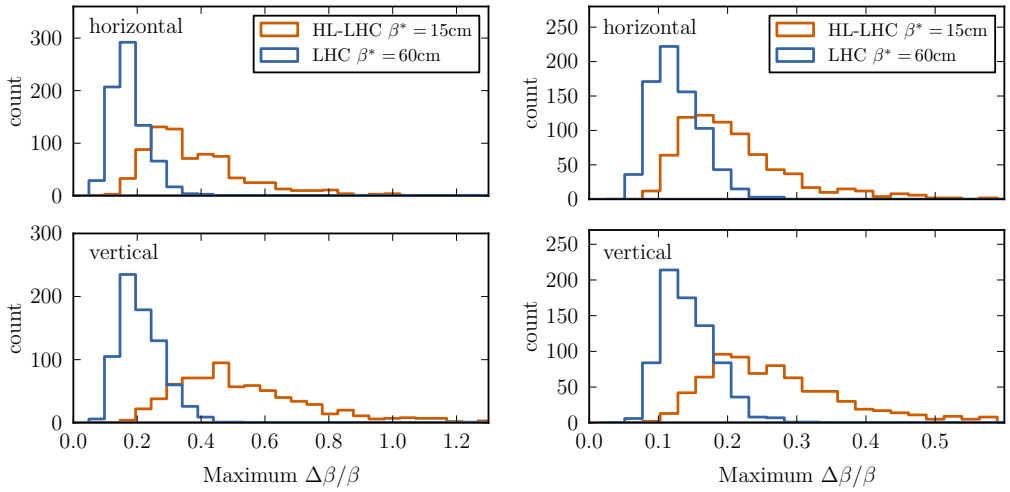

Figure 11: Peak horizontal (top) and vertical (bottom) β-beating distributions for LHC and HL-LHC before (left) and after (right) global optics correction neglecting triplet errors.

are tested via simulations. It is assumed that previous local correction would have successfully corrected errors of the final focusing triplet magnets and their errors are neglected.

10^3 lattices are simulated by randomly applying uncertainties , following a Gaussian distribution, truncated at three standard deviations. BPM measurement uncertainties are neglected in this study. The distribution of the resulting peak β-beating is shown in Fig. 11 (left). The peak β-beating distribution for the LHC is consistent with measurements after local corrections [4]. The resulting β-beating due to the optics perturbations is about a factor two to three worse for the HL-LHC. For each case a global optics correction is calculated, assuming no uncertainty of the phase advances. The peak β-beating distributions after the correction are shown in Fig. 11 (right).

After one iteration of global optics corrections, the HL-LHC peak β-beating is

a factor two worse than in LHC at about 20%. This is consistent with the observed 25% in the ATS optics measurements with arc β functions increased by a factor 4 as shown in Fig. 9. Note that corrections were computed at $\beta^* = 21$ cm [45, 46], leaving margin for improving the experimental result. Summarizing, in HL-LHC arc errors will contribute between 10% and 20% peak β-beating after local and global corrections, while in LHC this is closer to 5%. This takes the HL-LHC expected β-beating very close to the specified tolerances for LHC [49] and further improvements might be required to keep margins.

5 K-modulation in LHC and HL-LHC

Betatron functions at the Interaction Points (IPs) of the HL-LHC must be accurately controlled to maximize luminosity, but also to avoid significant imbalances between the experiments. The luminosity imbalance between the two largest experiments, ATLAS [50] and CMS [51], should not surpass 5% [4, 52] and thus dictates an accuracy on β^* measurements of about 2%. Currently, the preferred method to calculate β^* in the LHC is based on K-modulation of the last quadrupoles before the IP [14, 53, 54]. With K-modulation, the gradient of a quadrupole is modulated, and the induced tune shifts are measured to determine the average betatron function in that quadrupole. The average betatron functions in the triplets can be interpolated to the IP to calculate β^*. A more complete discussion of the theoretical background and methods can be found in [14].

K-modulation simulations were done in MAD-X for the HL-LHC optics at nominal injection tunes ($Q_x = 62.28$, $Q_y = 60.31$) to study the errors in β^* measurements. The results for the different optics were calculated using a version of the analytical method presented in [14] adapted for the split triplet quadrupoles closer to the IP and used in the HL-LHC. In Fig. 12 a sketch of the HL-LHC IR with split quadrupoles is presented. The use of injection tunes provides a larger tune separation compared to collision tunes thus allowing to use three times larger modulation amplitudes which significantly improves the accuracy of the β^* measurement. The uncertainty is determined by calculating the domain of β^* within the tune measurement uncertainties and determining the spread, $\frac{1}{2}(\beta^*_{max} - \beta^*_{min})$. Simulations in [16] show that the rms tune ripple coming from quadrupoles and dipoles power converter jitter in HL-LHC is expected to be $\delta Q = 4.1 \times 10^{-5}$ at β^*=15 cm. This value differs from [55, 56] as takes into account contributions from the arcs and new improvements in the triplet circuits and the power supply stability. However $\delta Q = 4.1 \times 10^{-5}$ gives a too large β^* measurement uncertainty of 7.7% and it has been proposed to upgrade the dipole power converters of the ATS arcs (A12, A45, A56 and A81) to class 0 [16]. With this upgrade the expected tune ripple is $\delta Q = 2.7 \times 10^{-5}$. In the following we assume that the

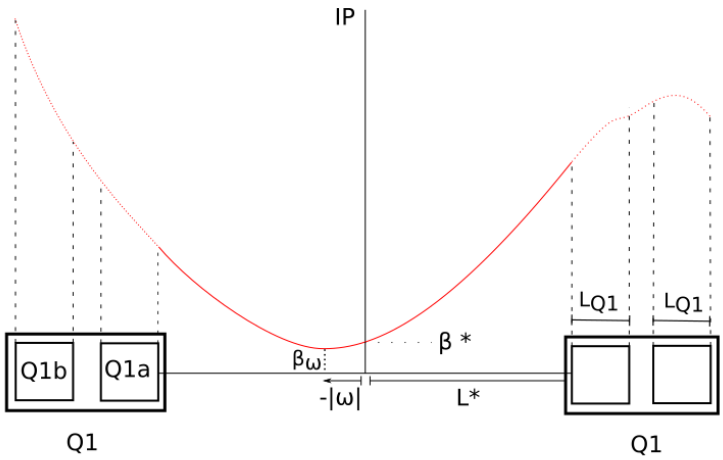

Figure 12: Schematic representation of the IR configuration. This corresponds to the default horizontal plane as defined in MAD-X models of the HL-LHC, with a focusing quadrupole on the right and a defocusing quadrupole on the left.

average tune measurement accuracy in HL-LHC is $\delta Q = 2.5 \times 10^{-5}$, slightly below the tune ripple. This requires the power converters upgrade and possibly the use of noise filters at the tune measurement level. The finite accuracy of the quadrupole gradient (δK) is considered as well. It was assumed that the two parts of one Q1 have the same uncertainty of 10 units. On top of that, each one has an uncertainty of 2 units. Longitudinal misalignment and manufacturing tolerances (δL^*) are also included in the simulations. Misalignments are assigned using a flat distribution with maximum deviations of ± 2 mm as estimated in [57].

Figure 13a shows the relative errors for β^* obtained of uncertainty for different HL-LHC IR optics. Presented in blue are the calculated errors for simulations assuming only an uncertainty in the tune measurement and without fringe fields. In black are the obtained errors when including fringe fields in the simulations. The implementation of fringe fields slightly increases the calculated errors on β^*. This effect is, however, only limited to 1% for the HL-LHC at the smallest optics. The data in red shows the errors when including contributions from the quadrupole powering (δK). In green misalignments of the split quadrupoles (δL^*) were added. Including all sources of error significantly increases the errors on β^* measurements to about 6% for the round $\beta^* = 15$ cm optics with $\delta Q = 2.5 \times 10^{-5}$. The presented simulations show, that the leading sources of error are the tune uncertainty δQ and the longitudinal misalignment δL^* highlighting the importance

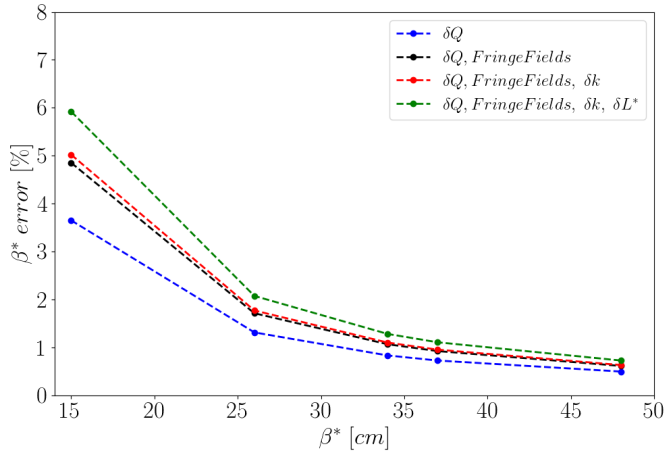

(a) Calculated errors when using both parts of the split Quadrupole

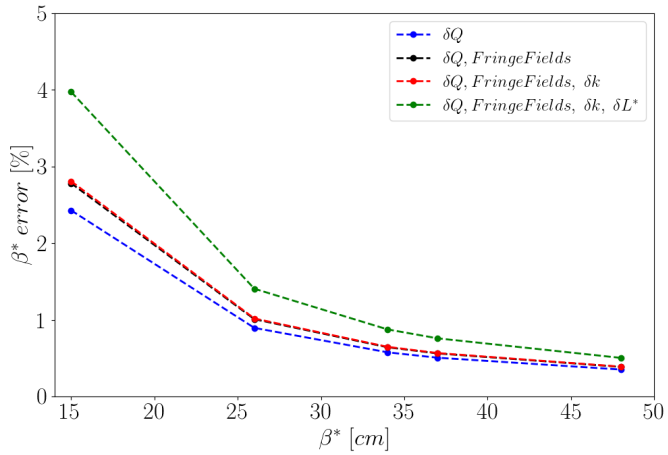

(b) Calculated errors when using only the innermost part of Q1

Figure 13: Calculated errors using the analytical method for different error contributions and for a range of HL-LHC optics. In blue are the errors found for simulations without fringe fields. Results adding fringe fields are shown in black, while errors found when adding uncertainties in K (0.1%) are shown in red. Adding longitudinal quadrupole misalignments, $\delta L^* = 2$ mm, results in the green curve.

of accurate tune measurements and reduction of the mechanical tolerances.

In the new baseline it is possible to only modulate the part of the split quadrupoles closer to the IP. This comes with a significant improvement in the accuracy of K-Modulation from 6% to 4% as shown in Fig. 13b.

Further sources of systematic errors such as influence of linear coupling and quadrupole tilts in the triplet have been studied in [14]. Their effect on β^* accuracy is below 1% assuming the coupling is well corrected to $|C^-| \leq 6 \times 10^{-4}$. Simulations with rms tilts in the Q1a and Q1b quadrupoles in the order of 1 mrad showed a negligible effect of the tilts on the IP optics calculations.

6 BPM calibration limitations

As a result of limitations of β from phase and K-modulation measurement techniques, the betatron amplitude is investigated to provide a measurement of β function along the IR. An analysis of the β from amplitude method is performed, to understand the impact of the individual BPM calibration factors and find optics-measured-based calibrations [63].

The methodology followed consists on the comparison of β from amplitude to the K-modulation and β from phase. Since the accuracy and precision of the methods depend on the optics settings, a selection of LHC configurations has been made for this comparison, namely:

- β^* = **40 cm**: This is the operational configuration in 2016 and 2017. AC dipole and K-modulation optics measurement are available [58, 6].
- **Van der Meer**: With a $\beta^* \approx 23$ m this optics is used for luminosity and emittance calibration purposes. AC dipole and K-modulation optics measurement are available.
- **Ballistic**: In this configuration the triplets are switched off [59]. Therefore the β measurements are not affected by the systematic errors of the quadrupoles. Only AC dipole measurements are available [60].
- β^* = **2500 m**: High-β^* optics are required to minimize the beam-divergence $\sqrt{\frac{\varepsilon}{\beta^*}}$ at the interaction point for measurements at small scattering angles. For this configuration both AC dipole and K-modulation measurements exist [61, 62].

From the direct measurement of the amplitude of the transverse oscillations it is possible to obtain the beta function. The equation describing the turn-by-turn motion at the i^{th} BPM is given by

$$x_i(N) = C_i \sqrt{\beta_{x,i} 2J_x} \sin(\mu_{x,i} + 2\pi Q_x N + \phi) \ , \tag{3}$$

where μ_x is the phase advance function, $2J_x$ is the action, ϕ is the initial phase, Q_x is the tune, N is the turn number and C_i is the individual calibration factor of each BPM. The main limitation of this method is given by the uncertainty on the BPM calibration, C_i. The starting point for the β from amplitude calculations is to quantify the action. In this first step two assumptions are made: the calibration factors are normally distributed and they are independent of the oscillation amplitude. First analyses show a negligible dependence of calibration on oscillation amplitude.

A large β-beating could lead to a wrong calculation of the action, therefore affecting the β measurements. The action is computed as

$$2J_x = \frac{1}{M}\sum_{i}^{M}\frac{(A_{x,i})^2}{\beta_{x,i}^m}\ , \tag{4}$$

where the $\beta_{x,i}^m$ is the β from the MAD-X model and the sum is restricted to the arc BPMs to avoid the effects of the different BPM types in the IRs. Simulations have been performed to evaluate how β from amplitude is affected by β-beating. Several MAD-X simulations of the Ballistic optics have been performed including different quadrupolar error sources and computing the average ratio $\left\langle \frac{\beta_{measured}-\beta_{model}}{\beta_{model}} \right\rangle$ around the machine versus the rms β-beating. A positive average implies that errors in the machine tend to increase the transverse average beam size and an overestimation of the action according to Eq. (4). Figure 14 shows the former ratio averaged over the seeds having the same binned rms β-beating versus the rms β-beating.

LHC has about 500 BPMs per plane and per beam. To have a first idea of the impact of the calibration factors in the final results, the monitors have been divided in two groups. The division has been done according to their location: triplets and arcs. In the arcs, the BPMs are button-type monitors and measure the position of each beam independently. On the other hand, the BPMs placed in the triplets are stripline-type monitors that measure the position and are also capable of distinguishing between counter rotating beams in the same beam pipe. Making a comparison between β from amplitude and β from phase, a different behavior is observed between arc and IR BPMs. The following β-beating ratio is analyzed,

$$\frac{\beta_{\text{amplitude}}-\beta_{\text{phase}}}{\beta_{\text{phase}}}\ . \tag{5}$$

Several optics configurations, including Ballistic, High-β^*, Van der Meer and $\beta^* = 40$ cm have been analyzed to quantify this deviation. The difference in terms of the error bar of β from phase is also computed. Table. 4 displays the relative differences for Beam 1. Triplet BPMs consistently give a smaller β from

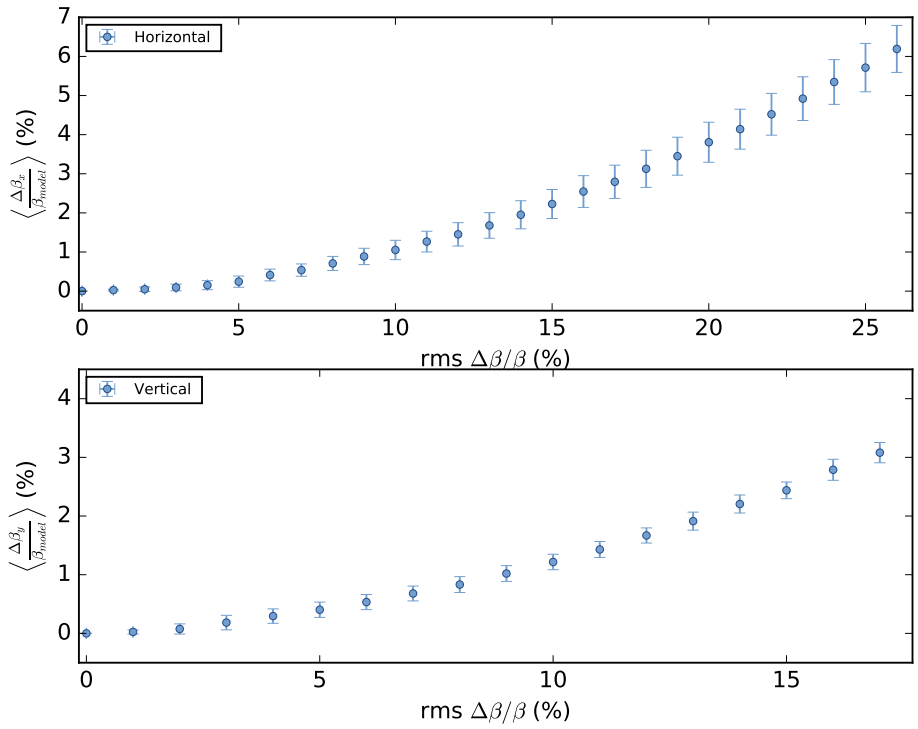

Figure 14: Average horizontal (top) and vertical (bottom) simulated β-beating around the machine and over the seeds having the same binned rms β-beating versus the rms β-beating. Error bars correspond to the standard deviation within a bin. Ballistic optics is used.

	Horizontal		Vertical	
BPM set	$\left\langle \frac{\Delta\beta}{\beta} \right\rangle$ [%]	$\left\langle \frac{\lvert\beta_{\text{amplitude}}-\beta_{\text{phase}}\rvert}{\sigma_{\text{phase}}} \right\rangle$	$\left\langle \frac{\Delta\beta}{\beta} \right\rangle$ [%]	$\left\langle \frac{\lvert\beta_{\text{amplitude}}-\beta_{\text{phase}}\rvert}{\sigma_{\text{phase}}} \right\rangle$
Arcs	0.83	4	-0.44	11
Inside triplets	-6.0	3	-6.9	4

Table 4: Deviation between β from amplitude and β from phase in relative terms, Eq. (5), and with respect to the error bar.

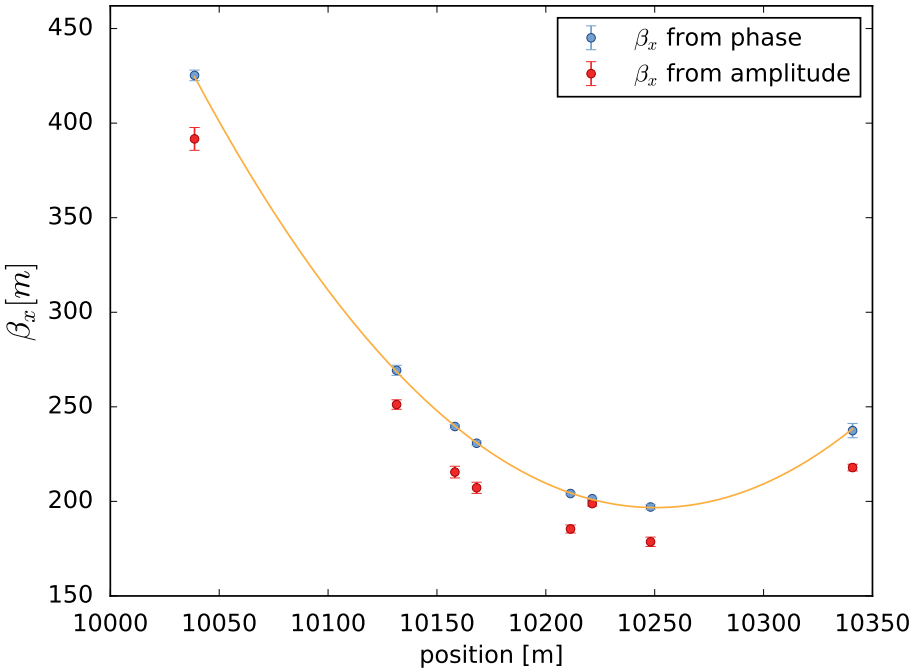

Figure 15: Measured horizontal β from amplitude and β from phase in IR5 for Beam 1. A parabolic fit to the β from phase measurement is also shown.

amplitude. Since the difference is significant in number of σ the calibration factor can be computed using β from phase as reference.

The first calibrations computed for LHC were obtained using the Ballistic configuration [60] from the MDs in November 2015 and March 2016. The procedure used to determine the BPM calibration factors is the following: (1) make a quadratic regression of the β function in the quadrupole free region, (2) obtain the values of the β with their error bars at the position of the BPMs and (3) compute the ratio $\frac{\beta_{\text{phase}}}{\beta_{\text{amplitude}}}$. An illustration in Fig. 15 shows β from amplitude being systematically lower than β from phase. The quality of the parabolic fit to the β from phase is remarkable.

To assess the effectiveness of the calibration factors computed with Ballistic optics, these have been applied to the high-β^* and nominal optics measurements. Table 5 illustrates the typical values of β from amplitude before and after the calibrations for $\beta^* = 2.5$ km. A general improvement in the measured β-beating from amplitude after applying the calibration factors can be observed for both optics. A histogram showing the calibrated β-beating with respect to the K-modulation data is shown in Fig. 16. The step histogram represents the β-beating after applying the calibration factors while the continuous line represents the non-calibrated

	Not calibrated		Cal. factors	Calibrated		Reference values	
BPM name	β_{amp} [m]	$\frac{\Delta\beta}{\beta_{\text{kmod}}}$[%]	C_i	β_{amp} [m]	$\frac{\Delta\beta}{\beta_{\text{kmod}}}$[%]	β_{phase} [m]	β_{kmod} [m]
1L5.B1	2374 ± 7	-7.3±0.3	1.11 ± 0.02	2644 ± 7	3±0.3	2576 ± 30	2562 ± 3
1R5.B1	2443 ± 5	-4.6±0.2	1.10 ± 0.01	2690 ± 6	5±0.2	2556 ± 30	2563 ± 2
1L1.B1	2171 ± 6	-11.3±0.3	1.03 ± 0.01	2237 ± 7	-8±0.3	2453 ± 50	2443 ± 1
1R1.B1	2254 ± 6	-7.7±0.3	1.03 ± 0.01	2331 ± 7	-5±0.3	2489 ± 60	2442 ± 2

Table 5: Calibrated and not calibrated horizontal β measurements for β^* = 2.5 km from Beam 1, using Ballistic calibration factors. β measurements from phase and K-modulation are shown as reference values.

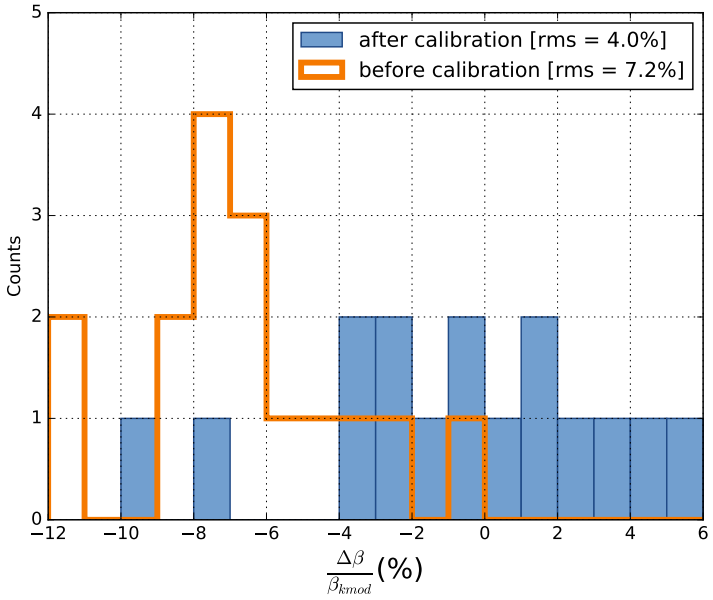

Figure 16: Overview of the effect of calibration factors

β-beating. The calibration has helped in centering the distribution and in reducing the rms deviation between β from amplitude and K-modulation from 7% to 4%.

7 HL-LHC IR local linear optics and coupling correction simulations

The HL-LHC aims to push β^* down to 15 cm in IP1 and IP5. This will increase the β-function in the triplet quadrupoles above 20 km, enhancing the impact of the triplet alignment errors and field quality in the machine optics.

The Q1 and Q3 quadrupoles of the HL-LHC are split into two magnets. This introduces two new sources of optics errors that have to be corrected using the

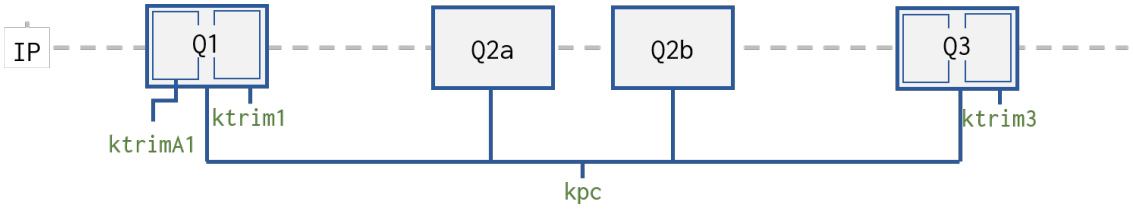

Figure 17: Schematic of the HL-LHC triplet and powering scheme [64]. The ktrimA1 is a 35 A circuit for K-modulation, see Section 5, and cannot be used for optics corrections.

same number of circuits as in the current LHC triplet, thus making the IR corrections more challenging than in the current LHC. Figure 17 sketches the HL-LHC triplet circuits.

Betatron phase advance is considered to be the most robust observable [2] to measure optics errors, but in regions with large β-function it becomes very small and, thus, very hard to measure. In these regions, like the LHC and HL-LHC high luminosity IRs, we rely on K-modulation which has allowed control of the β^* to 1% rms, as described in Section 2. Simulations have been performed for the HL-LHC to estimate the performance of this approach, assuming:

- Quadrupole gradient errors have an accuracy of 10 units (Gaussian distribution with sigma of $1‰$, equal in all quadrupoles in one seed) and a precision of 2 units, which varies between quadrupoles in the same seed. Quadrupole sorting is also assumed, i.e., pairing the quadrupole magnets within Q1 and Q3 with similar transfer function to minimize errors within the same circuit.
- ± 2 mm uniformly distributed longitudinal misalignments in each quadrupole of the triplet.
- phase advance measurement precision of $0.7 \times 10^{-3} 2\pi$ in the normal arc BPMs [6] and scaled according to $1/\sqrt{\beta}$ elsewhere.
- β-function measurement uncertainty of 0.48% in the BPMs closest to the IPs from K-modulation. This is the corresponding value to 4% precision in β^* from Section 5.

Triplet errors might cause the lattice to become unstable, so firstly just the segments around the IP1 and IP5 are simulated as individual beam lines (from the 12^{th} quadrupole on the left side to the 12^{th} quadrupole on the right side). A correction is computed for these sections only, using the Segment-by-segment technique as presented in Section 2. After an automatic local correction has been found, the errors with the corrections are introduced in the full ring to evaluate the residual β-beating. In Fig. 18 the maximum β-beating for 100 random seeds of

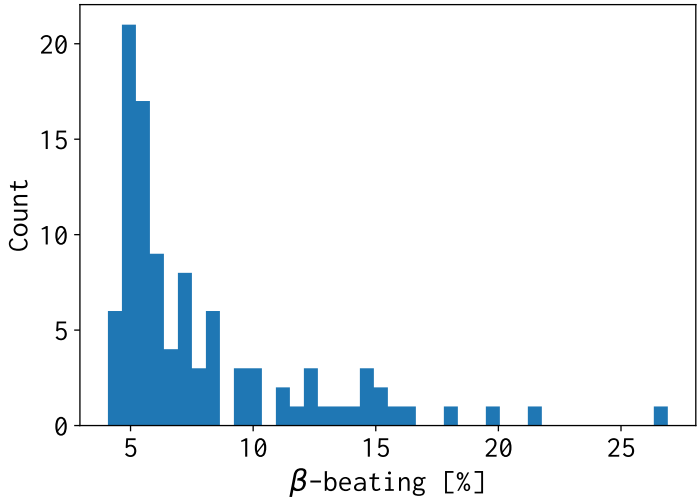

Figure 18: Simulated maximum β-beating for 100 simulations of the HL-LHC for 15cm round β^*. The average is 6.7% with an rms of 8.6%

the HL-LHC V1.2 sequence with 15 cm round optics is shown.

The maximum β-beating is generally located at the IPs along with waist shifts. The resulting rms β-beating of 8.6% is a factor 2 above the expected accuracy in the β^* measurement from K-modulation of 4%, but it is dominated by few seeds in the tail of the distribution (maximum 28%). These seeds should be analyzed to improve the correction algorithms.

Concerning the β functions at the crab cavities the performance of corrections is considerably better than at the IP. A maximum β-beating of 3.1% is expected at the crab cavities after correction.

The β-function measurements coming from calibrated β from amplitude could also be included in the segment-by-segment matching scripts, as it provides β measurements up to Q4 or Q5. However the current resolution of 4% shown in Section 6 should be improved before it makes a difference in the local corrections. Also, global corrections seem to have little effect in the final maximum β-beating. This should be closely analyzed as it disagrees with experience in the LHC.

Due to the very large β-function in the triplet, small tilts of the quadrupoles become very strong sources of linear coupling, while the tolerance for HL-LHC operation is set to $|C^-|0.001$ [17]. The segment-by-segment technique has been successfully used to correct such localized sources of coupling in the LHC. These corrections are performed by matching the difference coupling resonance driving term f_{1001} with the two available skew quadrupole correctors in the triplets. An

illustration is shown in Fig. 19a.

In the HL-LHC triplets we have 12 independent coupling sources per IR but only two local correctors. Local spikes of coupling are unavoidable as shown in Fig. 19b. As the $|C^-|$ depends on the global average of the f_{1001} driving term [7], these spikes have little impact on the closest tune approach.

Simulations over 100 machines with 0.5 mrad random Gaussian tilts in IR1 and IR5 triplet quadrupoles, Q4 and Q5 have been performed. The local quadrupole axes longitudinally have a maximum tilt of ± 2 mrad. The average tilt is measured with an accuracy of 0.5 mrad and the positioning accuracy is an order of magnitude better. An automatic correction was computed for IR1 and IR5, by fitting the f_{1001} driving term. A global correction was applied in the whole machine afterwards.

Figure 20 shows the expected $|C^-|$ after corrections for 100 random seeds, showing that the C^- is well suppressed below the tolerance of 10^{-3}. The MAD-X improvement in version 5.02.12 concerning the treatment of coupling made these results considerably better than previous simulations with older versions of MAD-X.

8 Effective optics modelling

Accurate modelling of a particle accelerator is crucial for its efficient and safe exploitation. It allows for rapid setup, performance optimization and predictions upon parameter changes. A beam-based or online model should be built to reproduce all available measurements, including the following ingredients:

- **Misalignments**: The most up-to-date survey data shall be included in the model. These are crucial for feed-down effects. In the LHC a dedicated application was implemented, which retrieves the relevant measurements from the databases and produces input to the MAD-X model.
- **Magnetic fields errors**: FiDeL model was developed to calculate the magnetic field imperfections for each magnet based on the powering history. Within the LHC beam-based model the FiDeL model is being implemented within a dedicated Java application. It calculates the magnetic errors at any moment on time and produces input for the MAD-X model.

  Even though magnets are measured accurately beam-based corrections are required. Systematic deviations coulbe be identified by combining measurements from different optics, e.g. nominal optics, ATS, the high-beta optics and the ballistic optics (where the triplet magnets were not powered).
- **Orbit**: A tool that incorporates the measured orbit into the model was implemented for the LHC. It introduces one virtual orbit corrector at the end

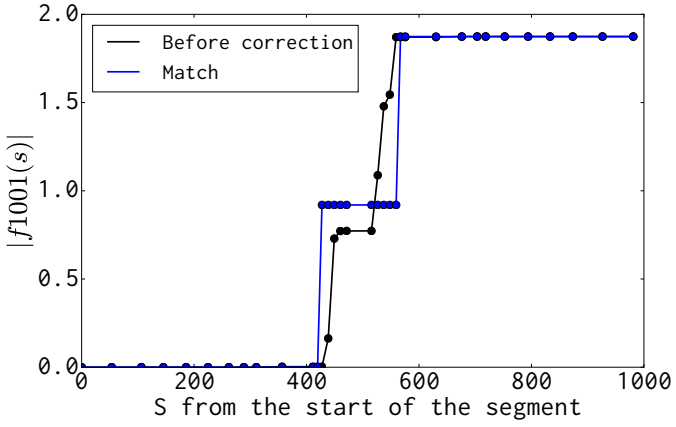

(a)

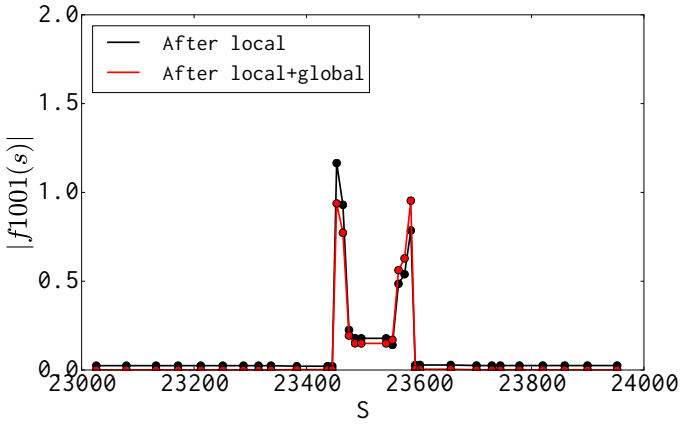

(b)

Figure 19: Segment-by-segment technique applied to the f_{1001} resonance driving term in HL-LHC. Figure (a) shows $|f_{1001}|$ before corrections simulating tilt errors in the triplet, Q4 and Q5 in black. The blue lines uses the two skew quadrupoles to match the f_{1001}. Figure (b) shows the effect of the correction, both after local (black) and local+global corrections (red).

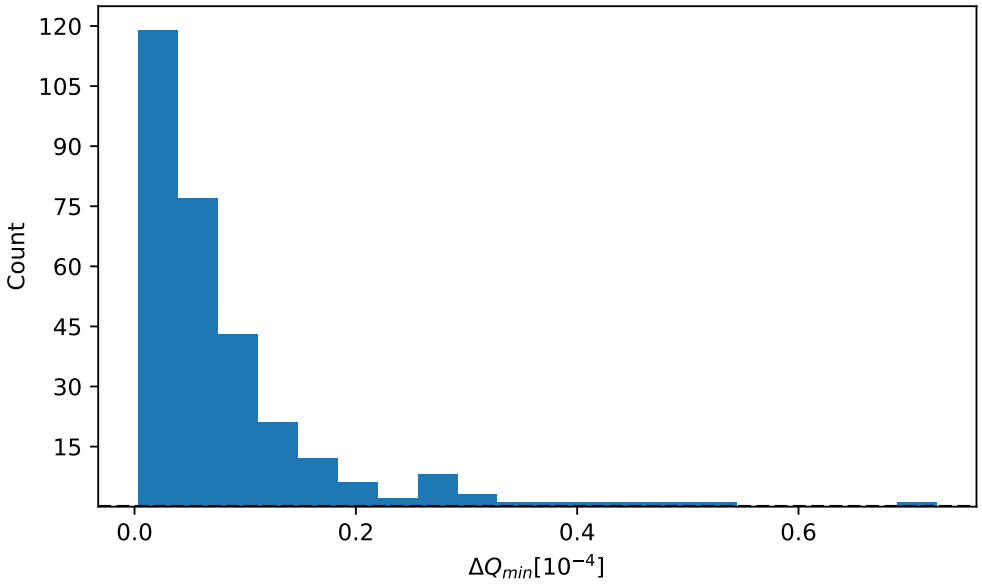

Figure 20: Closest tune approach in Beam 2 after local and global corrections for 0.5 mrad rms tilt errors in the IR quadrupoles. All the seeds are well below the 10^{-3} tolerance.

of every quadrupole and employs MAD-X orbit correction to reproduce the measurement. It was successfully verified in the LHC reaching a 0.1 mm deviation.

- **β-beating**: In the LHC the β function measurements are done with about 1% precision. The peak β-beating in LHC is about 5% and in the HL-LHC it may reach 10-20%. For many applications the most precise values of β function are required, e.g. emittance measurements or calculation of octupolar feed-down and its effect on tune. In the beam-based model a correction to each quadrupole in the lattice is calculated to reproduce the relevant phase advance measurement. A dedicated tool was implemented employing the algorithm of the optics corrections reproducing β functions within 1% accuracy.

A large part of the tools required to automatically build MAD-X models using magnetic measurements, LSA settings and measurements is already available. The constructed beam-based models and their predictive power need to be verified in the LHC. Experience on this front will be fundamental to address the HL-LHC challenges.

9 IR non-linear correction

As β^* is reduced the impact of nonlinear errors in experimental insertions becomes more significant. At $\beta^* = 40$ cm in the LHC, the operational impact of such nonlinearities was already becoming appreciable. The HL-LHC however, could potentially move to a regime where the IR nonlinear errors become a serious operational challenge. Ultimately this challenge may be regarded via the expected impact of the nonlinear errors on dynamic aperture. This problem has been studied extensively [65, 10], and from DA and lifetime issues alone it is expected that correction of the nonlinear errors in experimental insertions will be essential for the HL-LHC. Additionally however, a substantial impact of these errors may be expected on the accelerator optics. This is set to pose additional challenges to HL-LHC operation.

9.1 Theoretical use and expected performance of HL-LHC non-linear correctors

As is the case for the nominal LHC, a dedicated set of non-linear correctors are planned to be installed in the high-luminosity insertions to cope with the field quality of the single-aperture magnets. The correction strategy follows that established for correcting the field imperfections of the existing triplet and D1 [66]. The basic principles of the method are described below, with its extension to new multipoles such as a_5, b_5 and a_6 for which no correction is currently available in the nominal LHC.

On either side of the IP of the low-β insertion, generally in between the inner triplet and D1 where the β functions are substantially different in both planes, a dedicated correction coil is installed for each multipole component which is found to be critical for the DA. For the latest version of the HL-LHC optics and layout [10], the multipole correctors of the triplet and D1 are combined in a corrector package installed on the non-IP side of Q3, which contains all multipole magnets, normal and skew, up to order $n = 6$, except b_2 (see Fig. 21).

For a given normal or skew field imperfection $B_n^{\pm}(s)$ ($n = 2$ for quadrupole), generally varying from magnet to magnet, the correction consists in canceling one or more resonance driving terms, as seen by both beams, Beam1 and Beam2, namely

$$c_{1,2}^{\pm}(n;p,q) \stackrel{\text{def}}{=} \int_{\text{IR}} B_n^{\pm} \beta_{x_{1,2}}^{\frac{|p|}{2}} \beta_{y_{1,2}}^{\frac{|q|}{2}} e^{i\left(p\mu_{x_{1,2}} + q\mu_{y_{1,2}}\right)}, \tag{6}$$

where p and q are integers such that $|p| + |q| = n$, q is even (resp. odd) in the case of normal (resp. skew) multipole. Additional detail on the minimization proposed is given in Ref. [67].

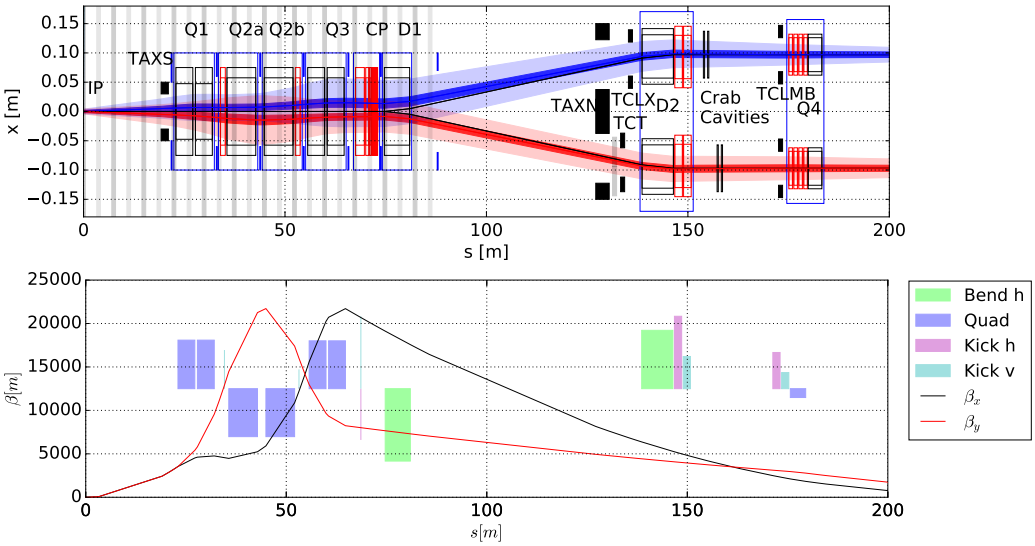

Figure 21: Upper: Overall layout of one side of the high luminosity insertion region between the IP and Q4. The non-linear correctors are located in the region marked CP. The dark blue and red areas represent the 2.4 σ beam envelope for the nominal round optics. The light regions correspond to a 14.2 σ value of the beam envelope. The vertical, shaded gray areas represent the locations of the parasitic beam-beam encounters. Lower: Evolution of the beta function in the insertion region for round optics configuration and $\beta^* = 15$ cm.

The specification of the strength requirements for the non-linear correctors has been performed by means of numerical simulations and depends on the field quality of the new triplet and D1 and details can be found in Ref. [10].

The performance of the proposed non-linear correctors has been assessed on the basis of numerical simulations of the dynamic aperture (DA) of the whole machine. The first results [67] were obtained for the SLHCV3.1b layout [68] and recently the situation has been re-assessed using the more recent HLLHCV1.0 optics version [10]. The main results are summarized in the Fig. 22, where the DA for 5 phase space angles, 60 seeds, 10^5 turns is shown. The field errors are assigned to all magnets in the arcs and IRs based on the data of the magnetic measurements. The markers represent the average DA (over the seeds and the angles), while the negative error bars represent the minimum DA (over the seeds and the angles) and the positive error bars the average DA over the angles of the maximum over the seeds. In this way the spread introduced by the realizations and the phase space angles is made visible in a compact form. In the upper plot the impact of each individual corrector is shown. It is worthwhile noting that for these simula-

tions the expected error tables are used, i.e., the field quality optimisation based on DA simulations is not applied. This is obtained by disabling all correctors in IR1 and 5 of a given multipolar order. The average DA is mainly affected by the b_3 corrector, while the minimum DA is more reduced by a_3, b_3 and b_6 correctors.

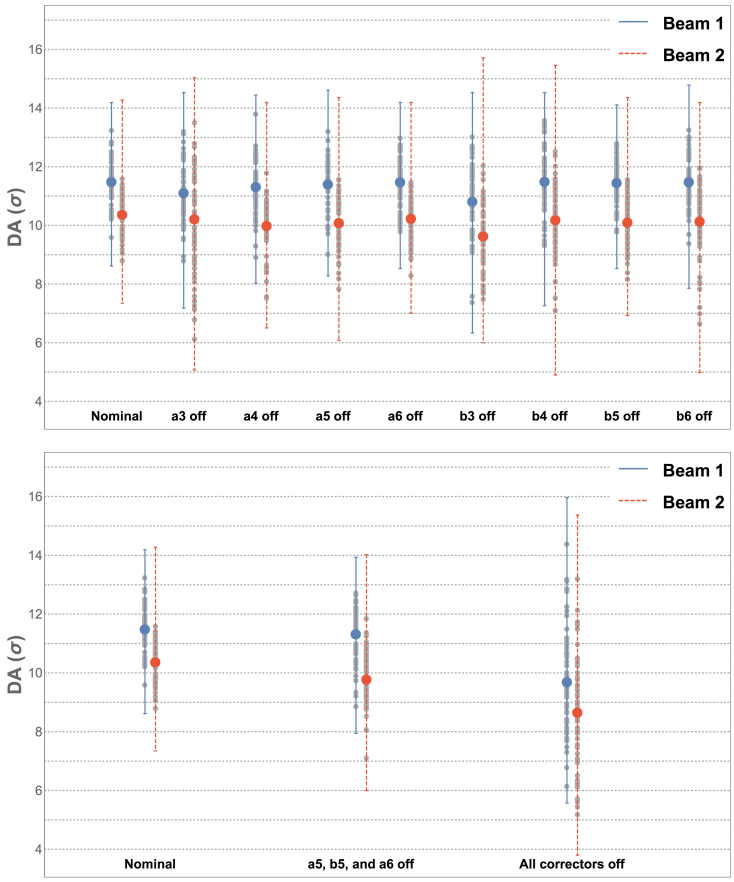

Figure 22: Impact of the absence of single corrector on dynamic aperture (upper). For each case shown, a corrector of a given multipolar order is disabled in both IRs. The impact of the absence of groups of correctors on dynamic aperture is also probed (lower). The dynamic aperture values are expressed using the nominal value of the normalized emittance, i.e., $\varepsilon_N = 2.5\ \mu$m.

In the lower plot the impact of the non-linear correctors is assessed. The extreme case in which these special correctors are switched off is considered and together with that a case in which only a_5, b_5, a_6 are switched off is evaluated. The latter represents a configuration similar to that of the nominal LHC, in which these tree corrector magnets are not installed. These two special configurations

are compared against the nominal one and the impact on the dynamic aperture is clearly seen. It is worth noting that the much larger effect of the correctors on the HL-LHC dynamic aperture reported in Ref. [67] is due to the choice of the configuration used for the numerical simulations. In fact, while the original simulations were performed assigning magnetic errors only to the triplet quadrupoles, the present results are obtained using the most detailed description of the HL-LHC ring, including all known magnetic errors.

Recently, the possibility of extending the function of the non-linear correctors to mitigate also for the impact of the field quality of the D2 separation dipole on DA has been explored. The fact that D2 has two apertures implies that only the average between the multipoles in the two apertures can be compensated for. This in turn implies that an effective correction can be expected only in the case of good correlation between the multipole components in the two apertures of the separation dipoles. This is indeed the case for the systematic multipoles, namely b_3 and b_5. Therefore, the original correction strategy has been extended by simply including the average b_3 from the D2 magnet.

The results are shown in Fig. 23, where the DA versus the systematic component of b_3 in the D2 is shown, for the case in which no correction is performed, i.e., the standard approach, or the one in which the functionality of the sextupolar corrector is extended. The results for both beams are reported.

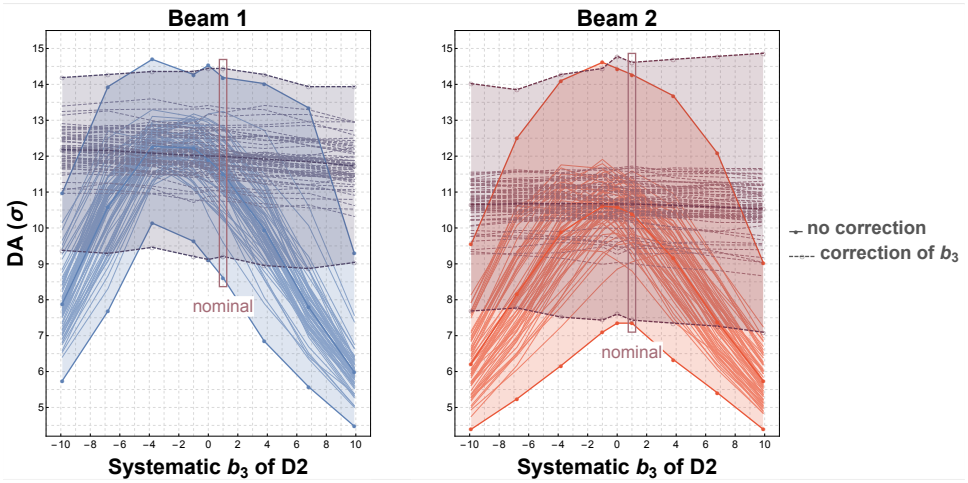

Figure 23: Dynamic aperture as a function of the systematic b_3 component in the D2 separation dipole without and with correction by the sextupolar magnet in the IT corrector package. Beam 1 (left) and Beam 2 (right) results are given. The dynamic aperture values are expressed using the nominal value of the normalized emittance, i.e., $\varepsilon_N = 2.5\ \mu$m.

The value of the nominal b_3 systematic component is highlighted for reference. The curves represent the minimum, average, and maximum over seeds and phase space angles. Moreover, the light lines represent the DA (averaged over the phase space angles) of the sixty seeds. The effectiveness of the correction strategy is clearly visible, and it improves for larger systematic b_3 component. This novel approach would be very useful in case of b_3 exceeding the expected value from electromagnetic simulations. For larger values of the systematic b_3 component the proposed correction strategy fails to be effective. This is probably due to compensation effects between the b_3 in the D2 separation dipole and similar components stemming from other magnet families. Another point worth consideration is the systematic difference in DA for Beam 1 and Beam 2: dedicated studies will be carried out to assess whether this is due to difference in phase advance between the various insertions for the two beams.

The next step is to consider the possibility to correct also the systematic b_5 component of D2. Preliminary results seem to indicate that the correction mechanism might not be as effective as for b_3 and the origin of the behavior is being investigated in detail.

9.2 LHC experience

Initial studies of IR-nonlinear errors in the LHC were performed during Run 1, utilizing feed-down to tune and linear coupling as a function of the IR crossing angle bumps [19]. These studies were used to validate the LHC magnetic model for several multipole errors, notably the b_3 component in IR2 and the b_3, b_4 and a_4 components of IR1 [19]. Figures 24 and 25 show examples of feed-down measurements where a good agreement was obtained between the measured data and predictions of simulations based upon the LHC magnetic model (WISE [69, 70]). Solid lines in the figures represent the predictions of WISE for 60 instances of the magnetic errors ('seeds'). In these cases corrections for the nonlinear errors can be calculated directly from the validated magnetic model.

Unfortunately feed-down studies on the LHC IRs have also revealed several instances of significant discrepancy between the beam-based measurements and the behavior predicted by the magnetic model. An example of such a measurement is shown in Fig. 26, where a discrepancy can be seen in the b_3 component of IR5 which feeds-down linearly to tune.

The observation that magnetic measurements during construction cannot be de facto relied upon to give an accurate description of the LHC behavior has serious implications for the correction strategy. It had previously been assumed that optimized corrections for the nonlinear errors could be calculated directly from magnetic measurements. In practice this is not the case. Beam-based methods for correction of the nonlinear errors will be essential in the HL-LHC.

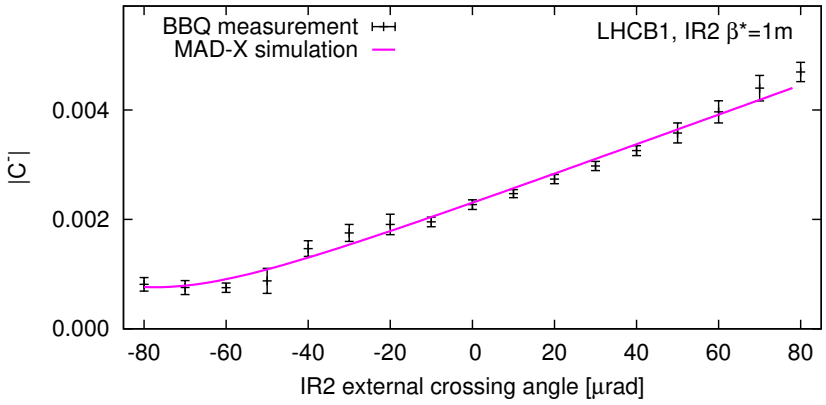

Figure 24: Modelled and measured feed-down to coupling with IR2 external crossing angle.

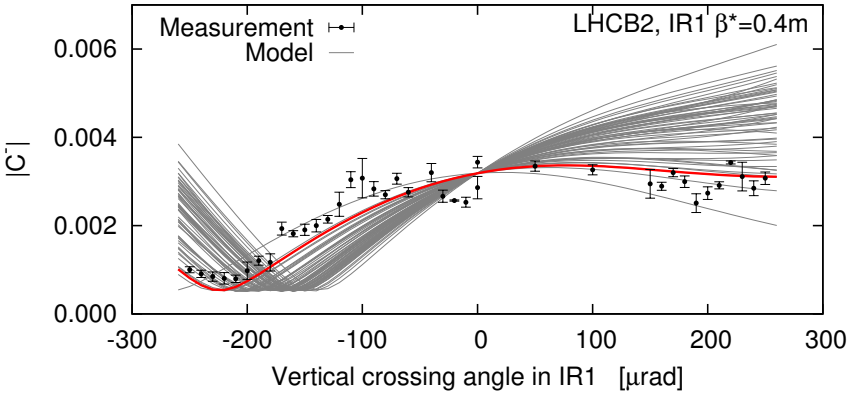

Figure 25: Modelled and measured feed-down to coupling with IR1 crossing angle.

In 2016 studies of the IR b_4 errors via feed-down were complemented by measurements of amplitude-detuning. Amplitude detuning provides a direct observable for the b_4 content of the machine, however measurement at high-energy only became viable late in Run 1 due to theoretical advances in understanding the detuning of driven oscillations in an accelerator [71, 72]. Figure 27 shows a comparison between the measured detuning and the expectation from the magnetic model. Cross-term detuning coefficients, which have very small values for this configuration of the LHC, are not shown. The measured detuning is dominated by the contribution from IR1 and IR5, and is seen to be $\sim 2/3$ of its nominal value.

Amplitude detuning effectively provides a measure of the total b_4 content of the ring weighted by β^2 at the location of the sources. To obtain a local correction it is necessary to identify the contributions coming from IR1 and IR5. In the case

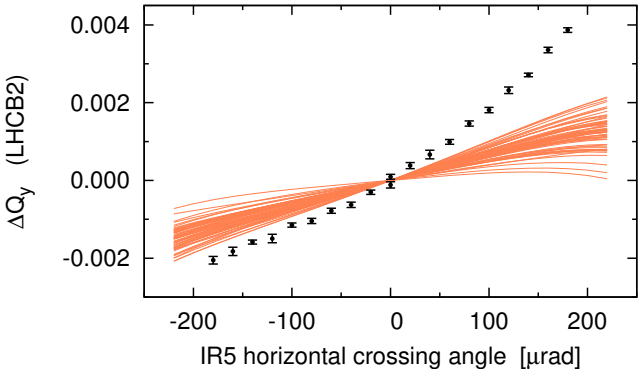

Figure 26: Modeled and measured feed-down to tune, as a function of the horizontal crossing angle in IR5.

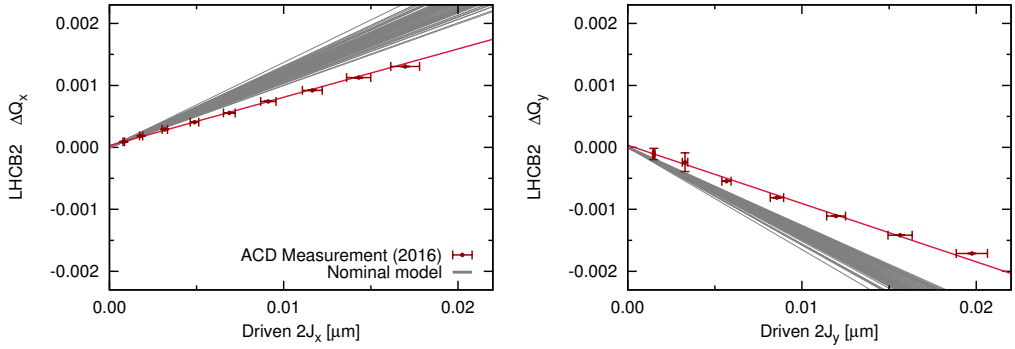

Figure 27: Measured amplitude detuning at $\beta^* = 40$ cm. PTC predictions based on the WISE model are shown in gray. Effects of driven oscillations have been accounted for in the comparison. The free amplitude detuning is obtained by dividing by 2 the plotted tune shift.

of IR1, crossing-angle scans demonstrated a good agreement for the second-order feed-down to tune generated by b_4. An example of this is shown in Fig. 28. The nominal b_4 correction, as determined from magnetic measurements, was therefore applied to IR1 (this correction had already been observed to minimize second-order tune feed-down from IR1 during 2012 [19]). The residual amplitude detuning was then minimized using the b_4 correctors in IR5. Application of both the IR1 and IR5 correction was observed to compensate the forced octupolar resonance driving term f'_{4000} as discussed in the following section. Application of the combined IR1 and IR5 correction was observed to significantly improve beam lifetime at $\beta^* = 14$ cm during an ATS MD in 2016 [45, 46], Fig. 29.

A beam-based correction of b_4 in the experimental insertions, calculated via

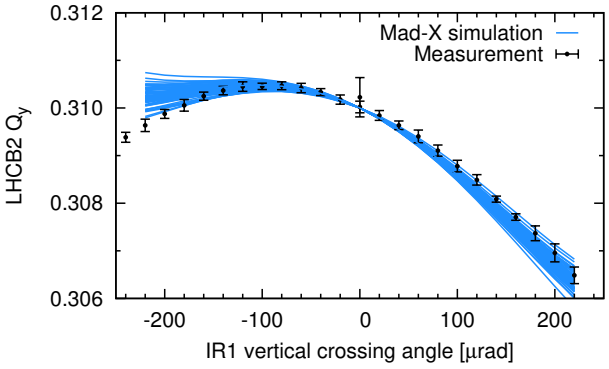

Figure 28: Simulated and measured variation of tune as a function of the vertical crossing angle in IR1. Effective a_3 settings were applied in simulation to reproduce the observed linear part of the tune variation, facilitating a comparison of the second-order feed-down from normal octupole errors.

feed-down and amplitude-detuning measurements, and validated through resonance driving terms and lifetime, has been demonstrated in the LHC. Feed-down studies have also been able to validate several other components of the magnetic model. Experimental results are being gathered in [18].

9.3 Effect of IR-nonlinearities on HL-LHC optics

Due to the reduced β^*, the impact of nonlinear errors in the experimental insertions of the HL-LHC can be expected to increase significantly compared to the LHC. The effect on the DA has been studied in detail [65, 10], however the impact on the optics may also represent a significant challenge. Simulations have been performed to examine the expected impact on the optics using the target error tables for the HL-LHCV1.0 (the same mask used for DA tolerance studies of the HL-LHC). 60 seeds of the errors are considered.

During operation for luminosity production a crossing scheme will be applied in the experimental IRs. As a consequence nonlinear errors will feed-down to generate linear optics perturbations. Figure 30 shows histograms over the target error table seeds, of the β-beating generated by normal and skew sextupole feed-down at $\beta^* = 15$ cm, with a 295 μrad crossing scheme. The peak β-beating is shown in blue, while the relative β^* imbalance is shown in red. With a peak $\Delta\beta/\beta > 20\,\%$, Fig. 30 demonstrates that the feed-down from IR sextupoles alone has the potential to violate machine protection limits in the HL-LHC. While most seeds examined did not exceed the maximum allowed β-beating on their own, many provided an insufficient margin of safety to accommodate residuals from the linear optics correction, and a potentially significant β-beating from beam-

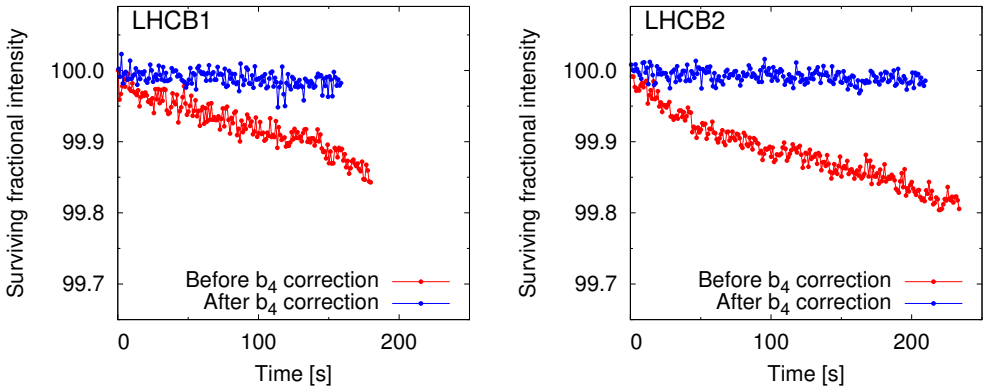

Figure 29: Surviving fractional intensity versus time, calculated from BCT data. The fractional intensity is calculated from ~ 2 minutes prior to application of the b_4 correction (blue), and for 2 minutes from the time of MCOX trim completion. The time period during which the b_4 correction is being applied is ignored, as feed-down to tune causes transient losses.

beam. Furthermore the β^* imbalance generated by the IR sextupoles in most cases is operationally intolerable.

Having the facility to compensate such errors will be essential for the HL-LHC, but may require a serious revision to the linear optics correction strategy. While application of nominal commissioning methods may be possible, in the LHC linear optics has always been commissioned with flat-orbit and correction with crossing scheme applied is entirely untested at low β. Furthermore, if crossing-angle bumps are to be varied during operation (to provide luminosity or pile-up leveling or to limit energy deposition in the triplets) changing feed-down will dynamically alter the β^*-imbalance during leveling unless local sextupole corrections are implemented.

Feed-down to coupling also represents a significant challenge. Figure 31 shows a histogram over the target error table seeds, of the linear coupling generated by sextupole feed-down alone for $\beta^* = 15$ cm, $295\,\mu$rad. Feed-down from the nonlinear errors in the experimental IRs has the potential to generate very large shifts to the linear coupling during the squeeze, up to 0.025. In the LHC $|C^-| \approx 0.004$ has been observed to cause instabilities and a tolerance of $|C^-| \leq 0.001$ is estimated for HL-LHC [17]. Therefore, correction of the IR coupling from feed-down during the squeeze will be essential. Further, allowing for a residual $|C^-|$ at the 10^{-3} level, the majority of seeds in Fig. 31 would generate enough coupling to cause HL-LHC beams to become unstable under the $\sim 60\,\mu$rad crossing-angle manipulations proposed for leveling during HL-LHC

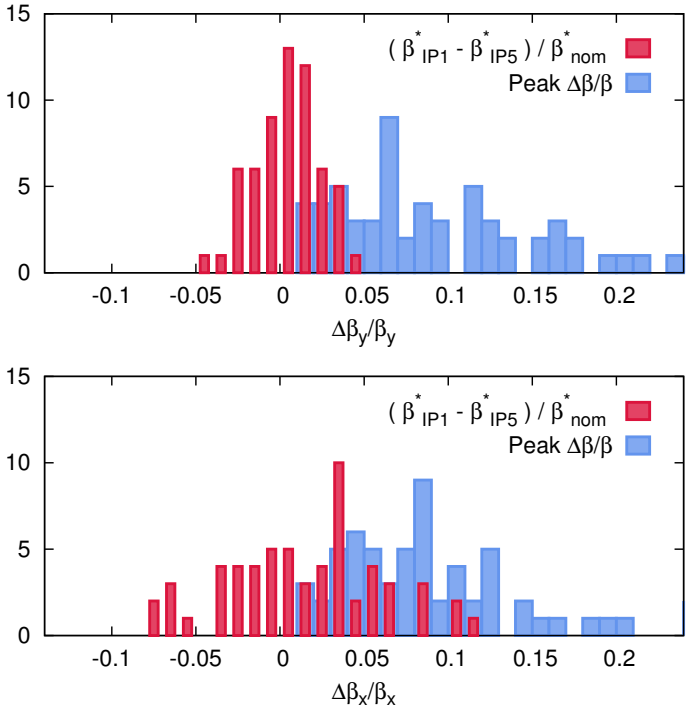

Figure 30: Predicted β-beating for 60 seeds of the HL-LHC target error tables at $\beta^* = 15$ cm, 295 μrad.

operation [73]. In this case local correction of normal and skew sextupoles in the IRs will become an operational necessity.

Perturbations to linear optics are not the only operational challenges which may arise from uncompensated nonlinear errors in experimental insertions. Distortion of tune footprint is also a significant issue due to the impact it may have on the Landau damping of instabilities.

To first-order in the multipole strength, normal octupole (b_4) fields generate first-order amplitude detuning: where 'first-order' here implies a linear tune shift with action ($J_{x,y}$, where $x = \sqrt{2\beta_x J_x}\cos\phi_x$). This contributes to the tune spread within a bunch, and therefore to the Landau damping. Landau octupoles in the LHC and HL-LHC arcs introduce such a tune-spread explicitly to provide Landau damping. As β^* is reduced however, the contribution to amplitude detuning arising from b_4 errors in the IRs increases. This distorts the intended tune footprint generated by the Landau octupoles, and leads to a tune spread which changes during the squeeze. Figure 32 shows the expected distortion of tune footprint during a nominal LHC squeeze, extrapolated from amplitude detuning measurements at $\beta^* = 40$ cm and 60 cm. Gray regions indicate the desired footprint, as generated by the Landau octupoles, and red regions indicate the footprint in the presence of

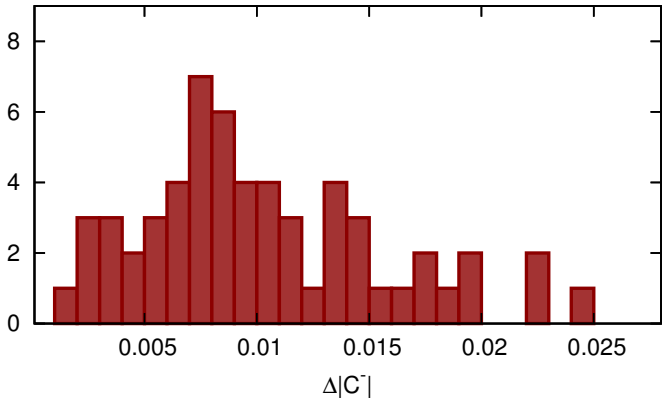

Figure 31: Histogram over HL-LHC target error table seeds, of the $|C^-|$ generated by sextupole feed-down only at $\beta^* = 15$ cm with the 295 μrad crossing scheme.

the measured b_4 errors.

At $\beta^* = 40$ cm in the LHC, the impact of normal octupole errors in experimental IRs has already been observed to impact upon the Landau damping of instabilities [74]. The impact in the HL-LHC is potentially far greater. Figure 33 shows histograms over the target error table seeds for the expected amplitude detuning in the HL-LHC generated by IR-octupole errors. Values measured in the LHC at 40 cm are also indicated.

The direct-term detuning coefficients ($\partial Q_x/\partial \varepsilon_x$ and $\partial Q_y/\partial \varepsilon_y$) of many seeds is increased substantially compared to the LHC at 40 cm. Significant cross-term detuning ($\partial Q_x/\partial \varepsilon_y = \partial Q_y/\partial \varepsilon_x$) is also generated in most seeds. In 2016 the Landau octupole settings in the LHC generated a magnitude of $\sim 110 \times 10^3\,\mathrm{m}^{-1}$ for the direct-terms and $\sim 80 \times 10^3\,\mathrm{m}^{-1}$ for the cross-term. In the HL-LHC, Landau octupole tune spread can be enhanced by the ATS telescopic squeeze: taking the maximum allowed current (570 A) the magnitude of the Landau octupole detuning at $\beta^* = 15$ cm is of the order of $\sim 300 \times 10^3\,\mathrm{m}^{-1}$ and $\sim 150 \times 10^3\,\mathrm{m}^{-1}$ for the direct and cross-terms respectively. By end-of-squeeze in the HL-LHC therefore, a significant proportion of the target error table seeds show octupole errors in the experimental insertions generating a tune spread larger than that created by the Landau octupoles during LHC operation. There is a serious risk therefore that uncompensated octupole errors in the HL-LHC experimental insertions will cancel or distort the tune footprint to the extent that Landau damping will be lost during the β^* squeeze. Furthermore, normal octupole errors are not the only source of footprint distortion arising from the low-β IRs: the orbit offset in the triplets and separation dipoles when the crossing scheme is applied during operation will

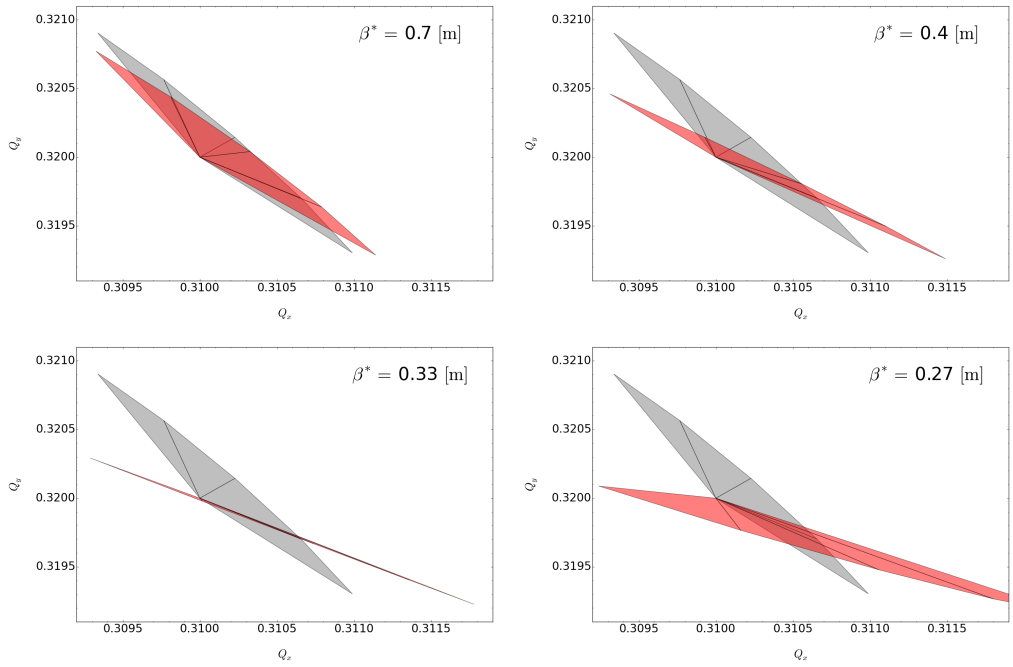

Figure 32: Distortion of tune footprint during a nominal LHC squeeze. Plotted footprints are defined by first-order detuning coefficients obtained via simulation with PTC_NORMAL. The model used consists of an effect model of the normal octupole errors in IR1 and IR5, which reproduces the observed detuning at $\beta^* = 40$ cm and 60 cm, together with Landau octupoles powered as per operation for Luminosity production in late 2016. Grey regions show the footprint expected in the absence of the IR contribution, red regions show the expected footprint in the real LHC if IR octupole errors are left uncompensated.

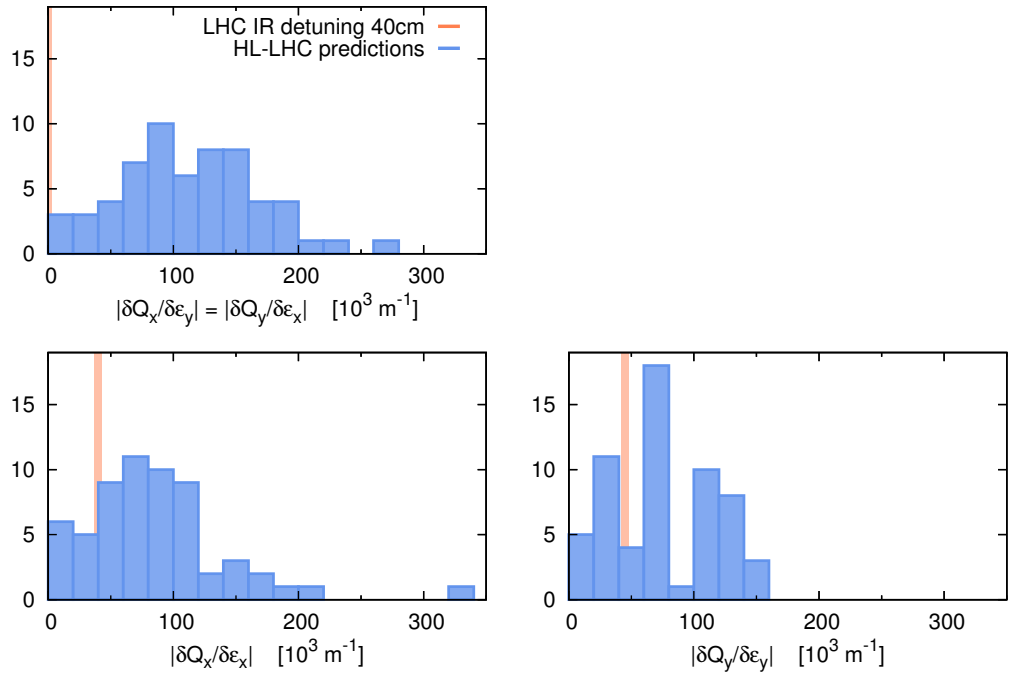

Figure 33: Histogram over target error table seeds for amplitude-detuning generated by IR-octupole errors in the HL-LHC at $\beta^* = 15$ cm, with a flat-orbit.

cause high-order errors, and in particular normal and skew decapole and normal dodecapole errors, to feed-down to normal octupole fields. Figure 34 shows histograms over the target error table seeds, of the change to the $\partial Q_y/\partial \varepsilon_y$ detuning coefficient resulting from only normal/skew decapole feed-down at $\beta^* = 15$ cm, $295\,\mu$rad.

On the upper end of the Fig. 34 histogram decapole feed-down can be expected to generate a tune footprint distortion on an operationally significant level. The situation becomes even more complicated upon addition of dodecapole feed-down. Figure 35 shows how the detuning coefficient of the first four target error table seeds change at $\beta^* = 15$ cm, as a function of the crossing angle in IR5.

Figure 35 shows that the tune footprint generated only by feed-down in experimental insertions of the HL-LHC can be larger than that generated operationally by the Landau octupoles in the LHC during 2016, and can be a significant fraction of the maximum tune spread from Landau octupoles in the HL-LHC. The exact form of the footprint, and hence the Landau damping, will depend on the interaction between the Landau octupoles, b_4, b_5, a_5 and b_6 errors in experimental insertions, with all having potentially significant contributions. For a given config-

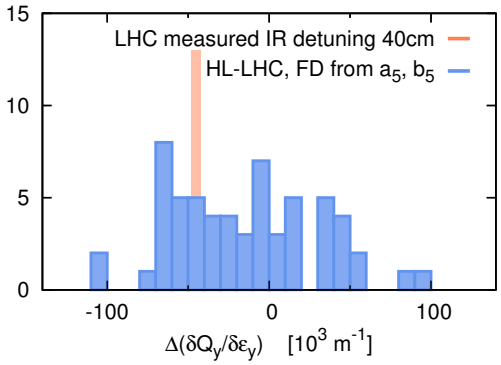

Figure 34: Histogram over target error table seeds for change in amplitude-detuning generated only by feed-down from normal and skew dodecapole errors in the HL-LHC at $\beta^* = 15$ cm, with a 295 μrad crossing scheme.

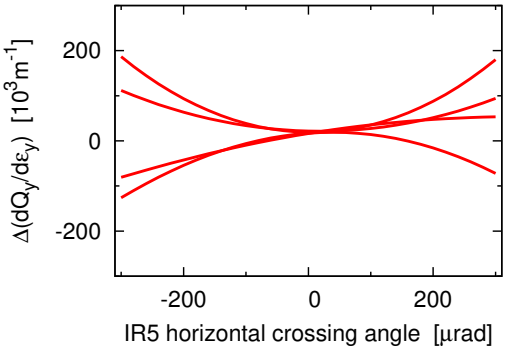

Figure 35: Change to the vertical detuning coefficient due to decapole and dodecapole feed-down in the first four seeds of the HL-LHC target error tables, as a function of the crossing angle in IR5 at $\beta^* = 15$ cm.

uration the impact of IR-nonlinearities may be more or less extreme, depending on crossing scheme, optics, and cancellation or enhancement between different IRs or multipole orders. However, the potential for significant distortion to tune footprint and Landau damping as a function of the the squeeze or the crossing scheme, makes local compensation of high-order IR errors an operational concern for the HL-LHC.

It will be very important to establish procedures for the linear and non-linear optics commissioning in the HL-LHC and identify possible limitations coming from increased non-linearity.

9.4 Correction methods in the HL-LHC

The HL-LHC will require robust methods for beam-based correction of the nonlinear errors in its experimental insertions. Two methods exist which may apply generally to a wide range of multipole errors. The measurement of resonance driving terms has the potential to allow for direct compensation of nonlinear sources in the IRs [75]. Spectral lines corresponding to normal and skew sextupoles and octupoles have been observed in the LHC. So far only octupolar resonance driving terms have been used to validate corrections in the LHC. Further details regarding driving terms measurements are given in Section 9.5. Some developments concerning the effect of the AC dipole and BPM calibrations are still required to reach full confidence.

Direct measurement of DA may also be a viable option. Conventional measurements based on single kicks are not possible at top energy due to the high rigidity of the beams and destructive nature of the measurement. However, the short term DA of driven oscillations can be studied using an AC-dipole. The short term DA is a new observable that can be used to benchmark models which also provides a lower boundary of the free DA, further details are discussed in Section 9.6. Long-term DA measurement can also be performed by blowing up the emittance with a transverse damper, and examining beam losses as a function of nonlinear corrector settings. This technique has been validated at injection in the LHC. First tests at top energy were also performed during MDs in 2016. Figure 36 shows clear changes to beam lifetime upon trims of the normal dodecapole correctors in the LHC. In the case shown, trims of b_6 correctors were applied to generate a shift to the dodecapolar detuning typical of that expected from the HL-LHC target error tables. A clear impact on beam-lifetime was observed indicating direct DA measurement should be viable in the HL-LHC. DA and lifetime are significant figures of merit for the IR correction quality which makes direct optimization of DA an appealing option for compensation of the IR errors, but given the global nature of such a measurement the challenge in its application will be separating contributions from different IRs and multipole orders. To this end DA must be complemented by methods based on study of the optics.

Regarding the sextupole-order errors, direct beam-based minimization of observed feed-down is a viable option, which should in principle compensate the operational impact arising from linear optics and coupling perturbations. On the downside, minimizing feed-down is unlikely to provide an optimal compensation of sextupole resonances, and may give less gains in dynamic aperture. It will be necessary to study this option further in simulation to help define correction priorities in the HL-LHC: it may be that the operational impact of β^* imbalance and coupling induced instabilities outweighs the need for an optimal resonance driving term correction. Methods based upon feed-down to tune and coupling

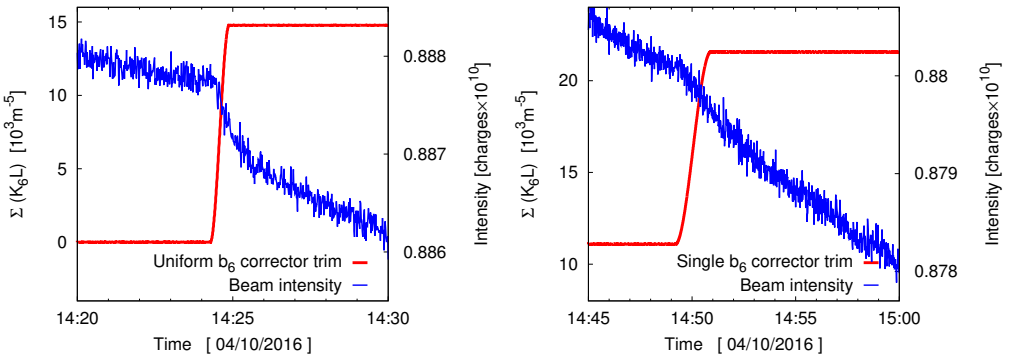

Figure 36: Measured intensity of LHC beams following uniform (left) and single corrector (right) trims to b_6 magnets in IR1 and IR5.

are relatively well established in the LHC for study of low-order nonlinear errors, and MD studies during 2016 have focused on improving the method further via better understanding and control of the orbit in the IR and its leakage to other IPs, improved coupling measurement, as well as through the use of an expanded repertoire of orbit bumps to probe specific regions of the IR [76].

In addition to these developments, the larger optics perturbations anticipated in the HL-LHC make additional methods viable. In particular it may be possible to adapt the segment-by-segment technique [2, 3, 77, 4], normally used for commissioning of local quadrupole corrections in LHC insertions, to the study of sextupole feed-down. Figure 6 shows error reconstruction via the segment-by-segment technique for LHC IR5 during 2016 optics commissioning. Figure 37 shows the phase advance discrepancy due to sextupole feed-down in the HL-LHC, as a function of the crossing scheme which is indicated in color. The seed considered corresponded approximately to the median of the β-beating distribution obtained for the target error tables, shown in Fig. 30. The order of magnitude of the phase advance discrepancy is comparable with that observed during 2016 LHC commissioning and, hence, easily measureble. Study of the local phase advance should better constrain potential sextupole sources than simple study of tune. A segment-by-segment method for sextupoles does appear to be of interest for the HL-LHC, however the method at present remains untested.

Compensation of IR-octupole errors has already been demonstrated in the LHC, with corrections determined via a combination of feed-down and amplitude detuning measurements. Such a combination of methods worked well in this case, however for b_4 errors it will always be possible to unambiguously compensate the detuning contribution from a given IR, by only squeezing one of the IPs. The challenge of the latter method arises in the overhead required to develop the single-IP squeeze, which may continue to make correction via a combination of

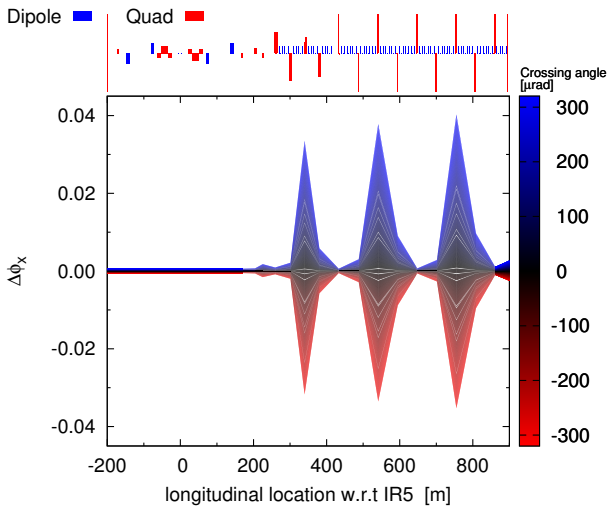

Figure 37: Segment-by-segment phase advance discrepancy due to sextupole feed-down in the HL-LHC. Crossing angle is indicated in colour.

techniques preferable. Errors of order greater than octupole can also be studied via their feed-down to amplitude detuning. First tests of this method were performed in the LHC during 2016 [76] and demonstrated it to be a challenging but potentially viable option for the study of high-order nonlinear errors.

In addition to feed-down to first-order detuning with amplitude, normal dodecapole errors directly generate second-order detuning (a quadratic variation of tune with action). Second-order detuning has been measured in the LHC at injection [78], but never observed at top energy. Second-order detuning from dodecapole sources in the experimental insertions scales with $\sim (1/\beta^*)^3$, and when measured via driven oscillations with an AC-dipole, direct second-order detuning coefficients are also enhanced by a factor 3 [71]. Given the small β^* in the HL-LHC it is possible for second-order detuning to become directly measurable. Figure 38 shows in red an example of a successful amplitude detuning measurement in the LHC at $\beta^* = 40$ cm. The range of actions plotted defines a realistically achievable measurement scenario, and the measured tune shift is representative of the scale on which we may be confident a precise measurement can be performed. Figure 38 also shows in blue, the expected tune variation with amplitude generated by the b_6 component of the 60 HL-LHC target error table seeds, including the factor 3 enhancement due to measurement with an AC-dipole. Given a realistically achievable range of actions, Fig. 38 demonstrates that in many seeds the predicted tune variation due to b_6, as measured by an AC-dipole in the HL-LHC at $\beta^* = 15$ cm, is comparable to successful detuning measurements performed in the LHC. Measurement of b_6 via second-order detuning at top energy remains

untested in a real machine, and may rely on accurate compensation of the lower-orders, but contrasting to the successful detuning measurements in the LHC it does seem that a direct measurement of b_6 may be viable.

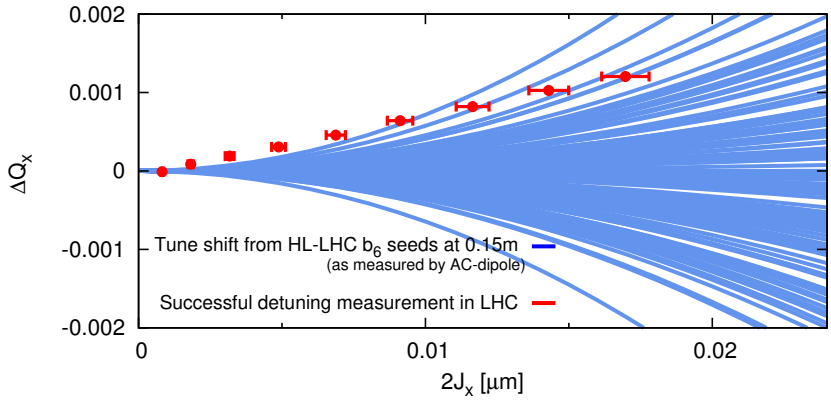

Figure 38: Red data shows an example of a successful measurement of amplitude detuning performed in the LHC at $\beta^* = 40$ cm. Blue lines show the predicted tune shift as a function of action due to the b_6 component of the 60 HL-LHC target error table seeds, including the factor 3 enhancement due to measurement with an AC-dipole.

Errors greater than dodecapole order are unlikely to have a significant effect on lifetime in the HL-LHC, and no correctors for such multipoles are planned. Still, study of the first-order feed-down to second-order detuning from decatettarapolar (14-polar) errors in the HL-LHC experimental insertions may be an interesting topic for an MD.

9.5 Resonance driving terms in LHC and HL-LHC

The measurement of Resonance driving terms (RDTs) is an effective method to probe machine nonlinearities. Spectral analysis of turn-by-turn data obtained from large transverse betatron excitations provides accurate measurements of the main tunes and secondary lines generated by various resonance driving terms. At top energy we rely on AC dipoles to generate non-destructive forced betatron oscillations [79]. The amplitudes of secondary lines in the spectra of forced oscillations are proportional to the sum of two RDTs of the same order [80], and can be used to identify different nonlinear sources [81].

Figure 39 shows the complex spectra obtained from turn-by-turn data at large diagonal excitaitons in Beam 2. All observable secondary lines are labeled according to $(m,n) = mQ_x^{AC} + nQ_y^{AC}$. The natural main tunes are labeled as N(1,0)

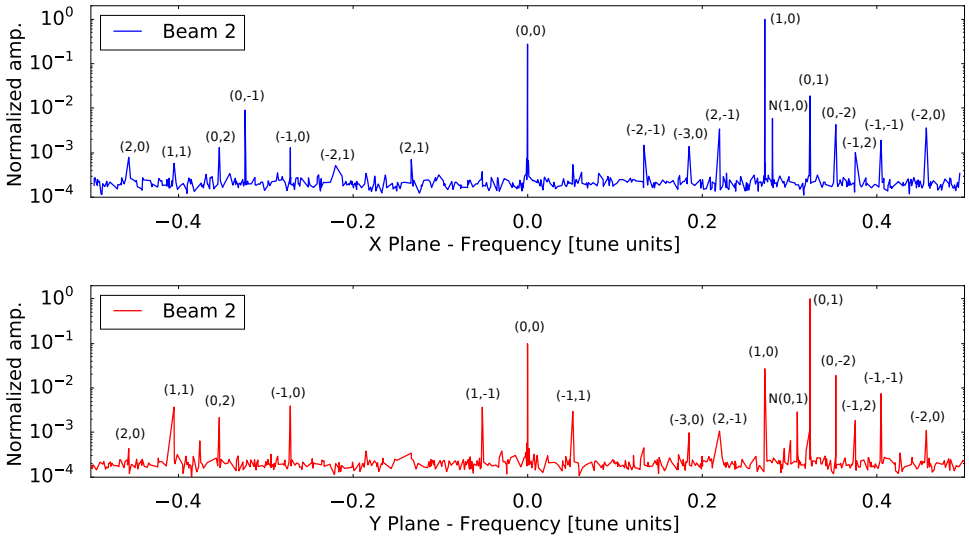

Figure 39: Complex spectrum of turn-by-turn data at large diagonal excitations in Beam 2. The lines observed are labeled according to $(m,n) = mQ_x^{AC} + nQ_y^{AC}$, while the natural tunes are given by N(1,0) and N(0,1).

and N(0,1) for the horizontal and vertical tune respectively. Figure 39 shows secondary spectral lines generated by normal and skew sextupoles and octupoles. Secondary lines arising from higher order multipoles have so far not been observed. Local nonlinear sources in the triplets will, however, be amplified in the HL-LHC due to the increased β functions and may improve measurements of such higher order sources.

Measurements of the normal octupolar RDT $|f'_{4000}|$ were used to confirm the correct implementation of b_4 corrections calculated from amplitude detuning measurements. Figure 40 shows a histogram of the measured RDT for all BPMs for three different measurements. In green the case where no b_4 corrections were applied, in orange only the corrections for IR1 were applied, and in purple corrections for both IR1 and IR5 were applied. A clear decrease in $|f'_{4000}|$ is observed after the implementation of each correction. Measurements of RDTs can thus be used to confirm the effectiveness of specific corrections and will be important to validate nonlinear correction schemes in the HL-LHC.

Measurements were done in 2016 to enhance specific RDTs by changing both the working point of the bare machine and the AC dipole to improve the resolution of RDT measurements. Normal and skew octupolar RDTs were enhanced successfully by approaching the generating resonances. Furthermore, this scheme may be envisaged to measure decapolar and dodecapolar RDTs that are currently

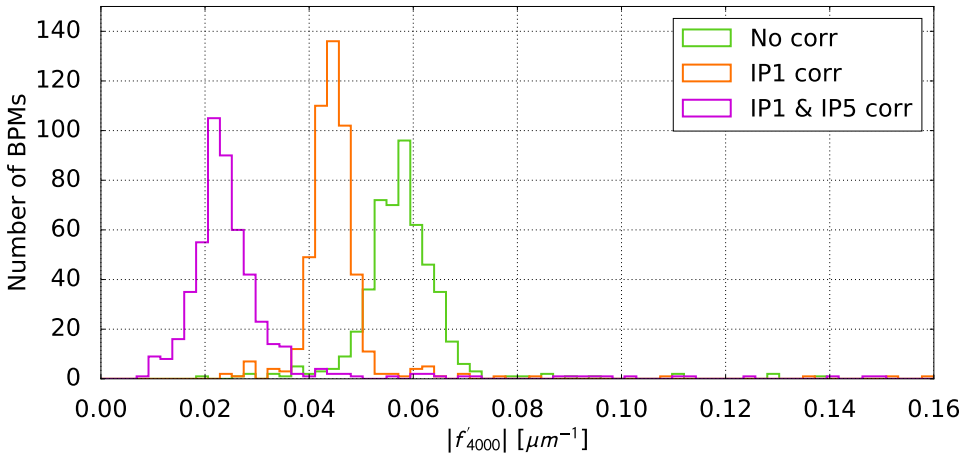

Figure 40: Histogram of the measured value of $|f'_{4000}|$ at each BPM. Green shows the measurement without b_4 corrections, orange shows the measurement with IP1 corrections, and in purple the measurement with b_4 corrections in both IP1 and IP5.

not observed. A scheme for nonlinear corrections can be devised for the HL-LHC where specific RDTs are probed through changes in the working point.

9.6 Short term DA with AC dipole

A new method to measure the DA under forced motion of an AC dipole, referred to as forced DA, has been proposed in [82] and envisaged as a complementary method in the HL-LHC alongside free DA measurements through beam heating. Measuring the forced DA allows to probe the nonlinear content of the machine by comparing to simulations.

The AC dipole excitation has the advantage of providing a slow ramp excitation that is considered safe at top energy. This allows to probe the forced DA at top energy in colliders where the single kick method is unviable. In the LHC the AC dipole is limited to an excitation of 10^4 turns while usual free DA studies consider measurements lasting an order of magnitude longer.

Particle dynamics under the driven motion of an AC dipole are considerably altered [80, 71, 72]. In general the number of resonances is larger when exciting the beam with an AC dipole. The choice of working point for the natural tunes as well as for the AC dipole tunes is therefore crucial to realize a representative forced DA measurement.

Resonances are approached through detuning with amplitude. As the oscilla-

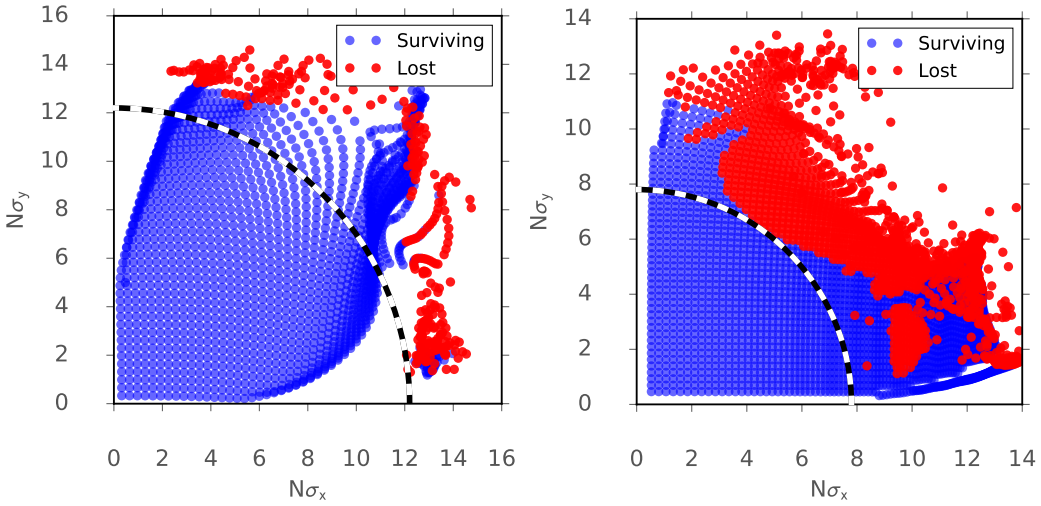

Figure 41: Comparison between DA simulations for LHC with single kicks (left) versus AC dipole (right). The machine tunes are $Q_x = 0.31$ and $Q_x = 0.32$, while the AC dipole tunes are $Q_x = 0.298$ and $Q_y = 0.335$. A clear reduction of measured DA is observed for the AC dipole simulations.

tion amplitude increases, the natural tunes will detune on to resonances causing particle losses. Amplitude detuning is in general larger with forced oscillations. It has been shown that the direct linear amplitude detuning terms generated by normal octupolar fields double under the influence of an AC dipole driven motion [71]. As such, resonances are predicted to be reached at lower actions than under free oscillation, likely reducing DA. The forced DA with AC dipoles could thus be viewed as a lower bound to free DA. Considerations on the influence of forced motion on forced DA are discussed in more detail in [83].

Figure 41 compares the free DA from simulations with single kicks with 8×10^3 turns to forced DA obtained from AC dipole tracking simulations at collision tunes ($Q_x = 0.31$, $Q_y = 0.32$), where a typical working point for the AC dipole is used; $Q_x^{\mathrm{AC}} = Q_x - 0.010$ and $Q_y^{\mathrm{AC}} = Q_y + 0.014$. The simulations are done at top energy at $\beta^* = 40$ cm m and without Landau octupoles. For single kicks the free DA is $12\,\sigma_{\mathrm{nom}}$, where σ_{nom} corresponds to $\varepsilon = 3.75\ \mu$m. A clear reduction is observed for AC dipole driven oscillations, where the forced DA is $8\ \sigma_{\mathrm{nom}}$. These results show a reduced forced DA for AC dipole excitations compared to the free DA, and offer a lower bound estimated of the free DA.

Measurements at injection energy were performed with the Landau octupoles powered at 40 A to probe this method. The measurements are discussed in greater detail in [83]. Figure 42 shows the measured beam losses for measurements at 40

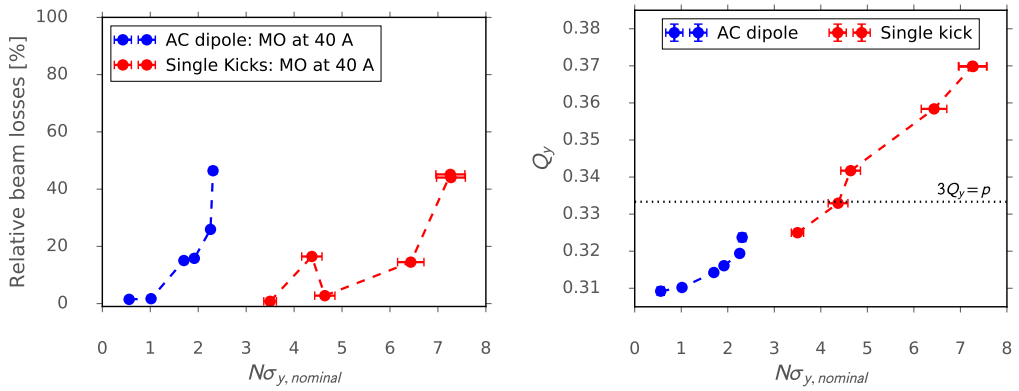

Figure 42: Measured natural vertical tunes versus. vertical excitation amplitudes for measurements with AC dipole (blue) and single kicks (red) and Landau octupoles powered at 40 A.

A with single kick and AC dipole in the vertical plane versus kick amplitude.

The short term forced DA was measured with the AC dipole at $2.3\,\sigma_{\mathrm{nom}}$ and was limited by the 3$^{\mathrm{rd}}$ order resonance $3Q_y = p$, as shown in Fig. 42. In the case of single kicks, the free DA arising from the 3$^{\mathrm{rd}}$ order resonance was limited to $4.3\,\sigma_{\mathrm{nom}}$.

10 Summary and outlook

HL-LHC represents a challenge for optics measurement and correction in both the linear and non-linear regimes. Fast and flexible tools will be required to efficiently commission the large amount of optics foreseen for the β^* leveling process. Algorithms are being developed and tested in the LHC to address these challenges. Table 6 collects the current relevant tolerances or expected values for optics parameters in LHC and HL-LHC. To reach 4% accuracy in HL-LHC β^* we are assuming the upgrade of the dipole power converters to class 0 in the telescopic arcs, which is not yet in the baseline [16]. Without this upgrade the tune jitter goes up to 4.1×10^{-5} and the β^* relative accuracy is 7.7%. Tune measurements in MDs during 2017 will allow characterizing power converter ripple.

Further developments are still required to guarantee a 2% accuracy in β^*. The LHC IR BPMs feature calibration errors in the 4% level. With optics-measurement-based calibration techniques, see Section 6, we have seen about a factor 2 improvement. BPM calibration errors of 1% in HL-LHC combined with optics-measurement-based calibration could help reaching the target of 2% accuracy in β^*.

	unit	LHC $\beta^* = 40$ cm	HL-LHC $\beta^* = 15$ cm
CMS/ATLAS luminosity imbalance tolerance	[%]	5	5
Tune jitter (rms)	$[10^{-5}]$	2-4	4.1
Assumed tune measurement uncertainty	$[10^{-5}]$	1.5	2.5
β^* accuracy:			
rms tolerance for lumi imbalance	[%]	2	2
rms achieved or expected	[%]	1	4
Peak β-beating after correction	[%]	5	10-20
β-beating from crossing angle (without non-linear IR correction)	[%]	2	20
$\lvert C^- \rvert$:			
Tolerance for instabilities	$[10^{-3}]$	1	1.0
Tolerance for K-modulation	$[10^{-3}]$	1	0.6
7 month drift	$[10^{-3}]$	3	12
$\Delta\lvert C^- \rvert$ from crossing angle (without non-linear IR correction)	$[10^{-3}]$	2	20
Dynamic aperture:			
Before IR correction	$[\sigma]$	10	5
After IR correction	$[\sigma]$	12	9

Table 6: Tolerances and achieved or expected values for LHC and HL-LHC optics control related parameters. Tune jitter values come from [16]. The assumed tune jitter of 2.5×10^{-5} requires upgraded power supplies for the telescopic arc dipoles. LHC DA values are taken from [84] and rescaled to the HL-LHC emittance of 2.5 μm.

Both experiments and simulations suggest that peak β-beating will be about 20% in HL-LHC, specially appearing in the arcs used for the telescopic squeeze.

The non-linear errors will pose severe challenges even for the linear optics commissioning via their feed-down to β-beating and coupling and by reducing the available DA for optics measurements with the AC dipole. Iterative corrections alternating the target between linear and non-linear orders will be required. A broad spectrum of techniques to measure and correct IR non-linear errors are emerging but a substantial effort is required to demonstrate their feasibility. A strategy based on these techniques should be defined and verified with simulations of realistic scenarios for optics commissioning in HL-LHC.

Acknowledgments

We are very thankful to Gianluigi Arduini for motivating this work and for proof-reading the manuscript. Research supported by the HL-LHC project.

References

[1] R. Tomás, M. Aiba, A. Franchi, and U. Iriso, *Review of linear optics measurement and correction for charged particle accelerators*, Phys. Rev. Accel. Beams **20**, 054801 (2017).

[2] M. Aiba, S. Fartoukh, A. Franchi, M. Giovannozzi, V. Kain, M. Lamont, R. Tomás, G. Vanbavinckhove, J. Wenninger, F. Zimmermann, R. Calaga, and A. Morita, *First β-beating measurement and optics analysis for the CERN Large Hadron Collider*, Phys. Rev. ST Accel. Beams **12**, 081002 (2009). http://journals.aps.org/prab/pdf/10.1103/PhysRevSTAB.12.081002

[3] R. Tomás, O. Brüning, M. Giovannozzi, P. Hagen, M. Lamont, F. Schmidt, G. Vanbavinckhove, M. Aiba, R. Calaga, and R. Miyamoto, *CERN Large Hadron Collider optics model, measurements, and corrections*, Phys. Rev. ST Accel. Beams **13**, 121004 (2010). http://journals.aps.org/prab/pdf/10.1103/PhysRevSTAB.13.121004

[4] R. Tomás, T. Bach, R. Calaga, A. Langner, Y. I. Levinsen, E. H. Maclean, T. H. B. Persson, P. K. Skowronski, M. Strzelczyk, G. Vanbavinckhove, and R. Miyamoto *Record low beta-beating in the LHC*, Phys. Rev. ST Accel. Beams **15**, 091001 (2012). http://journals.aps.org/prab/pdf/10.1103/PhysRevSTAB.15.091001

[5] A. Langner and R. Tomás, *Optics measurement algorithms and error analysis for the proton energy frontier*, Phys. Rev. ST Accel. Beams **18**, 031002 (2015).

[6] T. Persson, F. Carlier, J. Coello de Portugal, A. Garcia-Tabares Valdivieso, A. Langner, E.H. Maclean, L. Malina, P. Skowronski, B. Salvant, R. Tomas, and A.C. Garcia Bonilla, *LHC optics commissioning: A journey to the 1% optics control*, Phys. Rev. Accel. Beams **20** 061002 (2017) .

[7] T. Persson and R. Tomás, *Improved control of the betatron coupling in the Large Hadron Collide* Phys. Rev. ST Accel. Beams **17**, 051004 (2014).

[8] E.H. Maclean, F. Carlier, S. Fartoukh, T.H.B. Persson, J.M.C. Portugal, P.K. Skowronski, R. Tomás and D.A. Wierichs, *Demonstration of coupling correction below the per-mil limit in the LHC*, CERN-ACC-NOTE-2016-0053.

[9] T.H.B. Persson, Y.I. Levinsen, R. Tomás, E.H. Maclean, *Chromatic coupling correction in the Large Hadron Collider*, Phys. Rev. ST Accel. Beams **16**, 081003, 2013.

[10] *High-Luminosity Large Hadron Collider (HL-LHC) : Technical Design Report V. 0.1*, CERN-2017-007-M (2017). http://cds.cern.ch/record/2284929

[11] L. Medina and R. Tomás, *Performance and operational aspects of HL-LHC scenarios*, IPAC 2016, pp. 1516-1519. PerformanceandoperationalaspectsofHL-LHCscenarios

[12] L. Medina, R. Tomás and G. Arduini, *Studies on Luminous Region, Pile-up and Performance for HL-LHC Scenarios*, 8th Int. Particle Accelerator Conference 2017, pp. 1908-1911. http://accelconf.web.cern.ch/AccelConf/ipac2017/papers/tupik089.pdf

[13] L. Medina, R. Tomás and G. Arduini, *Effective pile-up density as a measure of the experimental data quality for High-Luminosity LHC operational scenarios*, submitted to Phys. Rev. Accel. and beams.

[14] F. Carlier and R. Tomás, *Accuracy & Feasibility of the β^* Measurement for LHC and HL-LHC using K-Modulation*, Phys. Rev. Accel. and Beams, **20**, 011005 (2017).

[15] J. Coello, *Minimum trim requirements and advantages of the single-circuit configuration*, in HL-LHC Magnet Circuits Internal Review 2017. https://indico.cern.ch/event/611018/timetable/

[16] D. Gamba, G. Arduini, R. De Maria, M. Giovannozzi, R. Tomás Garcia, J. Coello De Portugal, M. Cerqueira Bastos, M. Martino, *Beam dynamics requirements for HL-LHC electrical circuits*, to be published as CERN report (2017).

[17] E. Métral et al, *Update of the HL-LHC operational scenarios*, to be published, 2017.

[18] E.H. Maclean et al. *A new approach to LHC optics commissioning in the nonlinear era*, in preparation.

[19] E.H. Maclean, R. Tomás, M. Giovannozzi and T.H.B. Persson, *First measurement and correction of nonlinear errors in the experimental insertions of the CERN Large Hadron Collider*, Phys. Rev. ST Accel. Beams **18**, 121002 (2015).

[20] T. Pieloni, X. Buffat, L.E. Medina Medrano, C. Tambasco, R. Tomás, J. Barranco, P. Conclaves Jorge, C. Tambasco, *Dynamic Beta and Beta-Beating Effects in the Presence of the Beam-Beam Interactions* HB2016, Malmö,

Sweden.
https://hb2016.esss.se/prepress/papers/mopr027.pdf

[21] P. Gonçalves Jorge, J. Barranco, X. Buffat, F.S. Carlier, J.M. Coello de Portugal, E. Fol, L. Medina, T. Pieloni, R. Tomás, A. Wegscheider, *Measurement of Beta-Beating Due to Strong Head-on Beam-Beam Interactions in the LHC*, in 8th Int. Particle Accelerator Conference 2017, pp. 2121-2124.

[22] L. Medina, J. Barranco, X. Buffat, Y. Papaphilippou, T. Pieloni, and R. Tomás, *Correction of Beta-Beating Due to Beam-Beam for the LHC and Its Impact on Dynamic Aperture*, in 8th Int. Particle Accelerator Conference 2017, pp. 2512-2515. http://accelconf.web.cern.ch/AccelConf/ipac2017/papers/weoab2.pdf

[23] S. Fartoukh, *Achromatic telescopic squeezing scheme and its application to the LHC and its luminosity upgrade*, Phys. Rev. ST Accel. Beams **16**, 111002 (2013).

[24] M. Khun, V. Kain , A. Langner and R. Tomas , *First K-modulation measurements in the LHC during run 2*, IBIC 2015.

[25] J. Wenninger, *Update on IT movement in IR8*, LBOC Meeting No. 57. https://indico.cern.ch/event/506059/

[26] P.K. Skowronski, F. Carlier, J. Coello de Portugal, A. Garcia-Tabares Valdivieso, A. Langner, E.H. Maclean, L. Malina, T.H.B. Persson, B. Salvant, R. Tomás, *Limitations on Optics Measurements in the LHC*, IPAC 2016, Busan, Korea, pp. 3339-3342. https://cds.cern.ch/record/2207438/files/thpmb044.pdf

[27] R. Tomás, *On possible sources of luminosity differences between ATLAS and CMS*, Meeting No. 50. https://indico.cern.ch/event/451059/

[28] M. Kuhn, *Updated results from triplet K-modulation LBOC*, Meeting No. 52. https://indico.cern.ch/event/461647/

[29] T. Persson, *Beta* corrections strategies*, Meeting No. 52. https://indico.cern.ch/event/461647/

[30] P. Hagen, M. Giovannozzi, J.-P. Koutchouk, T. Risselada, S. Sanfilippo, E. Todesco and E. Wildner, *WISE: An adaptive simulation of the LHC optics*. Proc. EPAC06. Edinburgh, Scotland, 2006.

[31] P. Hagen, M. Giovannozzi, J.-P. Koutchouk, T. Risselada, F. Schmidt, E. Todesco and E. Wildner, *WISE: A simulation of the LHC optics including magnet geometrical data*, LHC Project Report 1123 (2008).

[32] S. Sanfilippo, P. Hagen, J.-P. Koutchouk, M. Giovannozzi and T. Risselada, *Transfer Function of the Quadrupoles and Beta-Beating*, LHC Project Workshop - Chamonix XV (2006), pp. 151-156.

[33] J. Coello de Portugal, F. Carlier, A. Garcia-Tabares, A. Langner, E.H.Maclean, L. Malina, T. Persson, P. Skowronski and R. Tomás , *Local optics corrections in the HL-LHC IR*, IPAC 2016, pp. 3480-3483. http://accelconf.web.cern.ch/accelconf/ipac2016/papers/thpmr040.pdf

[34] P. Castro, J. Borer, A. Burns, G. Morpurgo and R. Schmidt, *Betatron function measurement at LEP using the BOM 1000 turns facility*, PAC 1993, pp. 2103-2105.

[35] T. Persson, J. Coello de Portugal, M. Fjellstrom, L. Malina, J. Moeskops, G. Roy, P. Skowronski and A. Szczotka, *Review of the LHC Online Model Implementation and of its Applications*, IPAC 2016, pp. 1505-1508. http://cds.cern.ch/record/2207382/files/tupmw030.pdf

[36] J. Coello de Portugal, F. Carlier, A. Langner, T. Persson, P. Skowronski and R. Tomás, *OMC Software Improvements in 2014*, IPAC 2016, pp. 426-429. http://accelconf.web.cern.ch/AccelConf/IPAC2015/papers/mopje056.pdf

[37] R. Calaga, R. Miyamoto, R. Tomás and G. Vanbavinckhove, *Beta* measurement in the LHC based on K-modulation*, IPAC 2011, pp. 1864-1866. https://accelconf.web.cern.ch/accelconf/IPAC2011/papers/tupz027.pdf

[38] M. Kuhn, B. Dehning, V. Kain, R. Tomás, G. Trad, and R. Steinhagen, *New tools for K-modulation in the LHC*, Technical Report CERN-ACC-2014-0159 (2014).

[39] L. Malina, *Global Corrections*, OMC-meeting, CERN: https://indico.cern.ch/event/492736/contributions/2013393/attachments/1222214/1787392/Global_corrections.pdf

[40] R. Calaga and R. Tomás, *Statistical analysis of RHIC beam position monitors performance*, Phys. Rev. ST Accel. Beams **7**, 042801 (2004).

[41] A. Garcia, *IndiAna Jones and the Last Calibration*, https://indico.cern.ch/event/565942/contributions/2286215/attachments/1329277/1996886/presentation_AGTV_20160831.pdf

[42] P. Castro, *Luminosity and beta function measurement at the electron-positron collider ring LEP*, CERN-SL-96-070-BI.

[43] A. Franchi, *Error analysis of linear optics measurements via turn-by-turn beam position data in circular accelerators*, arXiv:1603.00281 [physics.acc-ph].

[44] A. Wegscheider, A. Langner, R. Tomás and A. Franchi, *Analytical N-BPM method*, submitted to Phys. Rev. Accel & Beams.

[45] S. Fartoukh, M. Albert, Y. Le Borgne, C. Bracco, R. Bruce and F. S. Carlier, J. M. Coello De Portugal - Martinez Vazquez, A. Garcia-Tabares Valdivieso, K. Fuchsberger R. Giachino, E. H. Maclean, L. Malina, A. Mereghetti, D. Mirarchi, D. Nisbet, L. Normann, G. Papotti, T. H. B. Persson, M. Pojer, L. Ponce, Laurette S. Redaelli, B. M. Salvachua Ferrando, P. K. Skowronski, M. Solfaroli Camillocci, R. Suykerbuyk, R. Tomas Garcia, D. Valuch, A. Wegscheider, J. Wenninger, *ATS MD's in 2016*, CERN-ACC-2017-0003 (2016). https://cds.cern.ch/record/2242513

[46] S. Fartoukh, R. Bruce, F. Carlier, J. Coello De Portugal, A. Garcia-Tabares, E. Maclean, L. Malina, A. Mereghetti, D. Mirarchi, T. Persson, M. Pojer, L. Ponce, S. Redaelli, B. Salvachua, P. Skowronski, M. Solfaroli, R. Tomaś, D. Valuch, A. Wegscheider, J. Wenninger, *Experimental validation of the Achromatic Telescopic Squeezing (ATS) scheme at the LHC*, IOP Conf. Series: Journal of Physics: Conf. Series **874** (2017) 012010.

[47] R. de Maria, S. Fartoukh, and M. Fitterer, *HLLHCV1.1: Optics Version for the HL-LHC Upgrade*. In Proceedings of IPAC 2015, Richmond VA, USA, 2015. https://jacowfs.jlab.org/conf/y15/ipac15/prepress/TUPTY037.PDF

[48] Y. Nosochkov, Y. Cai, M.-H. Wang, S. Fartoukh, M. Giovannozzi, R. de Maria, and E. Mcintosh. *Specification of Field Quality in the Interaction Region Magnets of the High Luminosity LHC Based on Dynamic Aperture*. In Proceedings of IPAC14, Dresden, Germany, 2014. http://www.slac.stanford.edu/cgi-wrap/getdoc/slac-pub-16023.pdf

[49] S. Fartoukh and O. Brüning, CERN-LHC-Project-Report-501, 2001.

[50] ATLAS collaboration homepage, http://atlas.web.cern.ch/Atlas/Collaboration/

[51] CMS collaboration homepage, http://cms.web.cern.ch/

[52] E. Meschi, ATLAS and CMS luminosity, LHC Machine Committee meeting, 2012.

[53] R. Calaga, R. Miyamoto, R. Tomas and G. Vanbavinckhove, *Beta* Measurement in the LHC Based on K-modulation*, Tech. Rep., CERN-ATS-2011-149, 2011.

[54] M. Kuhn, B. Dehning, V. Kain, R. Tomas, G. Trad and R. Steinhagen, *New tools for K-modulation in the LHC*, Tech. Rep., CERN-ACC-2014-0159, 2014.

[55] M. Fitterer, *Follow up of powering schemes for IT, q4 and d1/d2*, HL-LHC TC meeting, 2015.

[56] M. Fitterer, *Powering schemes for inner triplet, q4 and d1/d2*, HL-LHC TC meeting, 2015.

[57] E. Todesco, in 93rd WP2 meeting, https://indico.cern.ch/event/636344/

[58] A.S. Langner et al., *LHC optics commissioning at beta* 40 cm and 60 cm*, CERN-ACC-NOTE-2015-0035.

[59] *LHC Design Report*, CERN-2004-003-V-1 (2004).

[60] A. García-Tabarés Valdivieso et al., *MD Test of a Ballistic Optics* CERN-ACC-NOTE-2016-0008.

[61] H. Burkhardt, *High beta* optics*, In LHC Lumi Days: LHC Workshop on LHC Luminosity Calibration, http://indico.cern.ch/event/109784/timetable/#20110114.detailed

[62] A. García - Tabarés et al., *Optics measruements and corrections at $\beta^* = 2.5$ km*, to be published.

[63] A. García-Tabarés Valdivieso et al., *Optics-measurement-based BPM calibration*, Proceedings of 7th International Particle Accelerator Conference, Busan, Korea, pp. 3328-3331. https://cds.cern.ch/record/2207435

[64] F. Rodriguez, *4th HL-LHC TCC: State of discussion in preparation of circuit review*, https://indico.cern.ch/event/476960/.

[65] M. Giovannozzi, *Field quality and DA*. 6th HL-LHC Collaboration Meeting (14-16 November 2016, Paris, Espace St Martin). https://indico.cern.ch/event/549979/contributions/2263210/

[66] S. Fartoukh *et al.*, LHC Project Note 349, CERN.

[67] M. Giovannozzi, S. Fartoukh, R. De Maria, *Initial models of correction systems*, MILESTONE: M24.28. https://cds.cern.ch/record/1644776/files/CERN-ACC-2014-0010.pdf

[68] S. Fartoukh, R. De Maria, *Optics and Layout Solutions for HL-LHC with Large Aperture Nb3Sn and Nb-Ti Inner Triplets*, MOPPC011, Proc. IPAC12, p. 145.

[69] *WISE homepage*. http://wise.web.cern.ch/WISE/

[70] P. Hagen. *WISE - user guide and implementation notes*. http://wise.web.cern.ch/WISE/Doc/lhc-project-report-wise.pdf

[71] S. White, E. Maclean and R. Tomás. *Direct amplitude detuning measurement with ac dipole*, Phys. Rev. ST. Accel. Beams, **16**, 071002. http://prst-ab.aps.org/abstract/PRSTAB/v16/i7/e071002

[72] R. Tomás, X. Buffat, S. White, J. Barranco, P. Gonçalves Jorge and T. Pieloni, *Beam-beam amplitude detuning with forced oscillations*, Phys. Rev. Accel. and beams **20**, 101002 (2017).

[73] R. Tomás, *HL-LHC beam parameters for protons*. LHC Performance Workshop, Chamonix, 23-27 January, 2017. https://indico.cern.ch/event/580313/contributions/2359501/attachments/1399837/2139071/SLIDESlogo.pdf

[74] L.R. Carver, M. Schenk, R. De Maria, K. Li, D. Amorim, N. Biancacci, X. Buffat, E. Maclean, E. Metral, K. Lasocha, T. Lefevre, T. Levens and B. Salvant. *MD1831: Single Bunch Instabilities with Q" and Non-Linear Errors*, CERN-ACC-NOTE-2017-0012.

[75] M. Benedikt, A. Faus-Golfe, F. Schmidt, R. Tomas, P. Urschutz, *Driving Term Experiments at CERN*, Phys. Rev. ST Accel. Beams **10**, 034002 (2007)

[76] E.H. Maclean et al. *New methods for measurement of nonlinear errors in LHC experimental IRs and their application in the HL-LHC*, Proc. IPAC 17, Copenhagen, 3155-3158. http://accelconf.web.cern.ch/AccelConf/ipac2017/papers/wepik093.pdf

[77] G. Vanbavinckhove. *Optics measurements and corrections for colliders and other storage rings*. Ph.D. thesis, Universiteit van Amsterdam (2012). https://cds.cern.ch/record/1533084?ln

[78] E.H. Maclean, R. Tomás, F. Schmidt and T.H.B. Persson. *Measurement of LHC nonlinear observables using kicked beams*, Phys. Rev. ST. Accel. Beams, **17**, 081002. https://journals.aps.org/prstab/abstract/10.1103/PhysRevSTAB.17.081002

[79] R. Tomás, *Adiabaticity of the ramping process of an ac dipole*, Phys. Rev. ST Accel. Beams **8**, 024401 (2005). http://journals.aps.org/prab/pdf/10.1103/PhysRevSTAB.8.024401

[80] R. Tomás, *Normal Form of Particle Motion under the Influence of an AC Dipole*, Phys. Rev. ST Accel Beams, volume **5** 54001 (2002). http://journals.aps.org/prab/pdf/10.1103/PhysRevSTAB.5.054001

[81] R. Tomás, M. Bai, R. Calaga, W. Fischer, A. Franchi, and G. Rumolo, *Measurement of global and local resonance terms*, Phys. Rev. ST Accel. Beams **8**, issue 2, 024001 (2005). http://journals.aps.org/prab/pdf/10.1103/PhysRevSTAB.8.024001

[82] S. Mönig, E.H. Maclean, T.H.B. Persson, J. Coello de Portugal, A. Langner, R. Tomás, *Short term dynamic aperture with AC dipoles*, Proceedings of 7th International Particle Accelerator Conference, Busan, Korea, edited by C. Petit-Jean-Genaz, D. E. Kim, K. S. Kim, I. S. Ko, K. R. Kim, and V. RW Schaa, pp. 3496-3498 (2016) and CERN-ACC-NOTE-2015-0027 (2015). http://accelconf.web.cern.ch/AccelConf/ipac2016/papers/thpmr044.pdf

[83] F. Carlier, R. Tomás, E.H. Maclean, T.H.B. Persson, *First Experimental Demonstration of Dynamic Aperture Measurements under Forced Oscillation with an AC dipole*, submitted to Phys. Rev. accel. and beams 2017.

[84] R. Bruce, R. De Maria, M. Giovannozzi, D. Mirarchi and S. Redaelli, *MIN and MED optics final validation*, in LHC Machine Committee (LMC) March 2015. https://indico.cern.ch/event/377941